Supporting Information

Efficient and Low Roll-Off Solution-Processed Sky-Blue TADF Emitters via Hetero-Donor and Space Modification Strategies

Authors: Hao-Nan Shi,[a] Feng-Ming Xie,*[,a] Hao-Ze Li,[b] Yan-Qing Li,*[,b] Jian-Xin Tang*[,a,c]

[a] *Jiangsu Key Laboratory for Carbon-Based Functional Materials & Devices, Institute of Functional Nano & Soft Materials (FUNSOM), Soochow University, Suzhou, Jiangsu 215123 (P. R. China)*

[b] *School of Physics and Electronic Science, Ministry of Education Nanophotonics & Advanced Instrument Engineering Research Center, East China Normal University, Shanghai 200062 (P. R. China)*

[c] *Macao Institute of Materials Science and Engineering (MIMSE), Faculty of Innovation Engineering, Macau University of Science and Technology, Taipa, Macao 999078 (P. R. China)*

E-mail: fmxie@suda.edu.cn (F.-M. Xie), yqli@phy.ecnu.edu.cn (Y.-Q. Li), jxtang@must.edu.mo (J.-X. Tang)

Table of Contents

luminance of the device.

Table S1. Crystal data and structure refinement for HCB-1.

Table S2. Crystal data and structure refinement for HCB-2.

Table S3. Crystal data and structure refinement for HCB-3.

Table S4. Photophysical characteristics of HCB-1, HCB-2, and HCB-3.

Table S5. Photophysical characteristics of HCB-1, HCB-2, and HCB-3 in 100 wt% films.

Table S6. OLEDs performance based on HCB-1.

Table S7. OLEDs performance based on HCB-2.

Table S8. OLEDs performance based on HCB-3.

Table S9. EL performances of the reported blue and sky blue TADF-OLEDs by solution process.

Table S10. EL performances of the reported blue and sky blue TADF-OLEDs for vacuum-deposited devices.

Synthesis and characterization

Chemical Synthesis: All the reagents purchased from commercial sources were used without further purification. All the reactions were performed under nitrogen atmosphere, and the crude products were purified by column chromatography before characterizations and device fabrication.

Measurements and Characterization: The chemical structures were determined by ^{1}H and ^{13}C nuclear magnetic resonance (NMR) spectra with Bruker AVANCE III type NMR Spectrometer in $CDCl_3$ solution, Matrix-assisted laser desorption/ionization time-of-flight (MALDI-TOF) mass spectrometer, Elemental analysis test using Vario Micro cube elemental analyzer. and single-crystal X-ray diffraction. Ultraviolet–visible (UV-Vis) absorption and photoluminescence (PL) spectra were recorded at room temperature with a Perkin-Elmer Lambda 750 UV-Vis spectrophotometer and a FM-4 type fluorescence spectrophotometer (JY company, French), respectively. The optical bandgap (E_g) was determined from the onset of the absorption spectra. Low-temperature phosphorescence spectra were measured with a FLS 920 spectrometer (Einburgh Corporation) in neat film at 77 K. The absolute photoluminescence quantum yields (PLQYs) of the doped and non-doped films were obtained with a C9920-02G type fluorescence spectrophotometer (HAMAMASTU, Japan) with an integrating sphere at room temperature under nitrogen atmosphere.

Theoretical Calculations: All the quantum chemical calculations were performed using a DFT method in Gaussian 09 program package. The ground-state geometries were optimized by using a TD-DFT approach at the B3LYP/6-311G(d,p) level. The singlet and triplet excited-state properties were calculated according to the optimized geometries.

Cyclic voltammetry measurements: The HOMO and LUMO levels were determined from the Cyclic voltammetry (CV) measurements. CV measurements were conducted on a RST 3100 electrochemical analysis equipment at room temperature with a conventional three electrode configuration, consisting of a platinum disk working electrode, a platinum wire counter electrode, a Ag/AgCl reference electrode, and the supporting electrolyte of tetrabutylammonium hexafluorophosphate (0.1 M). The cyclic

voltammograms were obtained at a scanning rate of 50 mV s^{-1} with DCM solution.

Thermal properties: Thermal gravimetric analysis (TGA) was carried out with an HCT-2 instrument at a heating rate of 10 °C min^{-1} under nitrogen atmosphere.

Device Fabrication and Measurements: OLEDs were fabricated on the patterned indium-tin-oxide (ITO)-coated glass substrates with a sheet resistance of ~15 Ω per square. The ITO-coated glass substrates were successively cleaned in an ultrasonic bath with acetone, ethanol, and deionized water, and then dried in an oven at 110 °C. After the UV-ozone treatment for 15 minutes, the ITO-coated glass substrates were transferred into a high-vacuum deposition chamber (base pressure ≤ 2×10^{-6} mbar) for the thermal deposition of organic materials and metal electrodes through a shadow mask. After the film depositions, the fabricated devices were transferred to the nitrogen-filled glovebox for the encapsulation with a glass cap and epoxy glue. Current density-voltage-luminance (J-V-L) characteristics and EL spectra of the devices were measured simultaneously with a source meter (Keithley model 2400) and a luminance meter/spectrometer (PhotoResearch PR670). The CIE 1931 colour coordinates were obtained from the EL spectra. Low-temperature probe and semiconductor parameter analyzer for impedance measurement.

General information

The solvents used and the raw materials for synthesis were from commercial sources and directly used without any further purification.

Synthesis of materials

Synthesis of (2r,3s,5s,6s)-4'-(tert-butyl)-3,5-di(9H-carbazol-9-yl)-2,6-bis(3,6-di-tert-butyl-9H-carbazol-9-yl)-[1,1'-biphenyl]-4-carbonitrile (HCB-1).

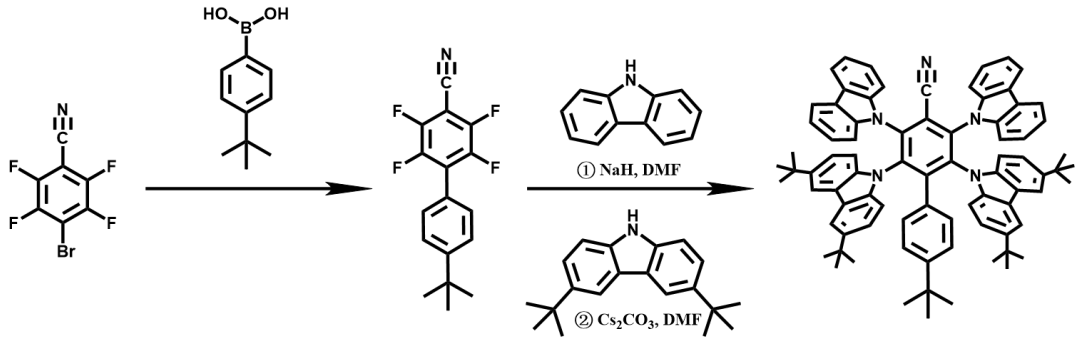

Scheme S1. The synthetic route of HCB-1.

Step (1): Compound 4-bromo-2,3,5,6-tetrafluorobenzonitrile (1.0 g, 3.9 mmol) and (4-(tert-butyl)phenyl)boronic acid (0.85 g, 4.7 mmol) were dissolved in 40 mL 1,4-Dioxane. Then $Pd[P(Ph)_3]_4$ (5% equi) and K_3CO_3 (1.1 g, 7.9 mmol) dissolved in water (3.7 ml) were added in a nitrogen atmosphere After the solution was heated at 105 °C for 18 hours, the reaction mixture was cooled to room temperature. The crude product was further purified by column chromatography on silica gel (DCM: hexane=1:4) to give 0.92 g (yield: 77%) of 4'-(tert-butyl)-2,3,5,6-tetrafluoro-[1,1'-biphenyl]-4-carbonitrile as a white powder.

Step (2): Carbazole (1 g, 5.7 mmol) and NaH (0.25 g, 10.0 mmol) were stirred for 30 min in N, N- Dimethylformamide (25 mL) in three-neck bottle under nitrogen at 0 ℃.Then compound 4'-(tert-butyl)-2,3,5,6-tetrafluoro-[1,1'-biphenyl]-4-carbonitrile (0.8 g 2.6 mmol) which dissolved in 35 mL dry N, N- Dimethylformamide was injected into the bottle and the reaction mixture was stirred 24 h at room temperature. Then, 3,6-di-tert-butyl-9H-carbazole (1.64 g, 5.8 mmol), Cs_2CO_3 (2.6 g, 7.8 mmol) and dry N, N-Dimethylformamide (30 ml) were added into the mixture. After the reaction mixture was stirred under N_2 atmosphere at 150 °C for 24 h. The mixture solution was poured into 250 mL water, and the green precipitates was collected by filtration under a reduced pressure. The crude product was further purified by column chromatography on silica gel (DCM: hexane=1:4) to give 1.18 g (yield: 53%) of **(2r,3s,5s,6s)-4'-(tert-butyl)-**

3,5-di(9H-carbazol-9-yl)-2,6-bis(3,6-di-tert-butyl-9H-carbazol-9-yl)-[1,1'-biphenyl]-4-carbonitrile as a green powder. ^{1}H NMR (400 MHz, $CDCl_3$) δ 7.69 – 7.64 (m, 4H), 7.52 (t, J = 1.8 Hz, 4H), 7.15 (dt, J = 7.6, 1.7 Hz, 4H), 7.05 (ddt, J = 6.8, 4.3, 1.4 Hz, 8H), 6.92 (dt, J = 8.6, 1.8 Hz, 4H), 6.84 (dd, J = 8.6, 1.8 Hz, 4H), 6.78 (dd, J = 8.5, 1.6 Hz, 2H), 6.54 – 6.50 (m, 2H), 1.31 (d, J = 1.5 Hz, 36H), 0.78 (d, J = 1.3 Hz, 9H). ^{13}C NMR (101 MHz, $CDCl_3$) δ 151.30, 151.01, 142.85, 140.61, 139.48, 137.75, 137.55, 130.00, 127.75, 125.06, 124.43, 124.03, 123.53, 122.31, 120.61, 119.80, 117.14, 115.35, 112.91, 110.40, 109.68, 34.44, 34.11, 31.84, 30.67. MALDI-TOF-MS (m/z) of $C_{81}H_{77}N_5$ for [M]+: calcd. 1120.202; found, 1120.542.

Synthesis of (2r,3s,5s,6s)-3,5-di(9H-carbazol-9-yl)-2,6-bis(3,6-di-tert-butyl-9H-carbazol-9-yl)-[1,1':4',1''-terphenyl]-4-carbonitrile (HCB-2).

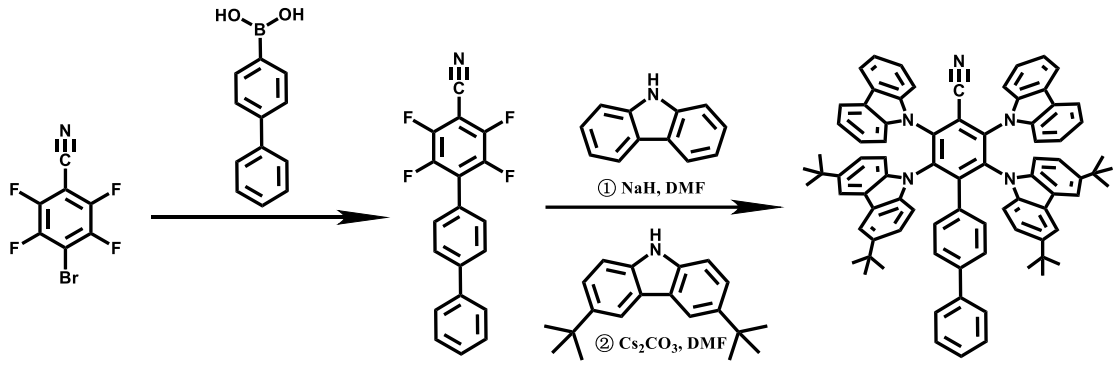

Scheme S2. Synthesis of HCB-2.

Step (1): Compound 4-bromo-2,3,5,6-tetrafluorobenzonitrile (1.0 g, 3.9 mmol) and [1,1'-biphenyl]-4-ylboronic acid (0.93 g, 4.7 mmol) acid were dissolved in 40 mL 1,4-Dioxane. Then $Pd[P(Ph)_3]_4$ (5% equi) and K_3CO_3 (1.1 g, 7.9 mmol) dissolved in water (3.7 ml) were added in a nitrogen atmosphere After the solution was heated at 105 °C for 18 hours, the reaction mixture was cooled to room temperature. The crude product was further purified by column chromatography on silica gel (DCM: hexane=1:4) to give 1.03 g (yield: 78%) of 2,3,5,6-tetrafluoro-[1,1':4',1''-terphenyl]-4-carbonitrile as a white powder.

Step (2): Carbazole (1.16 g, 6.9 mmol) and NaH (0.27 g, 11.5 mmol) were stirred for 30 min in N, N- Dimethylformamide (25 mL) in three-neck bottle under nitrogen at

0 ℃.Then compound 2,3,5,6-tetrafluoro-[1,1':4',1''-terphenyl]-4-carbonitrile (0.9 g 2.7 mmol) which dissolved in 35 mL dry N, N-Dimethylformamide was injected into the bottle and the reaction mixture was stirred 24 h at room temperature. Then, 3,6-di-tert-butyl-9H-carbazole (2.0 g, 7.1 mmol), Cs_2CO_3 (3.2 g, 9.8 mmol) and dry N, N-Dimethylformamide (30 ml) were added into the mixture. After the reaction mixture was stirred under N_2 atmosphere at 150 °C for 24 h. The mixture solution was poured into 250 mL water, and the green precipitates was collected by filtration under a reduced pressure. The crude product was further purified by column chromatography on silica gel (DCM: hexane=1:4) to give 1.21 g (yield: 51%) of **(2r,3s,5s,6s)-3,5-di(9H-carbazol-9-yl)-2,6-bis(3,6-di-tert-butyl-9H-carbazol-9-yl)-[1,1':4',1''-terphenyl]-4-carbonitrile** as a green powder. ^{1}H NMR (400 MHz, $CDCl_3$) δ 7.63 (dt, J = 7.0, 1.7 Hz, 4H), 7.48 (d, J = 1.8 Hz, 4H), 7.11 (ddt, J = 9.5, 6.3, 1.7 Hz, 7H), 7.07 – 6.98 (m, 10H), 6.97 – 6.89 (m, 6H), 6.85 (dd, J = 8.6, 1.6 Hz, 4H), 6.79 – 6.74 (m, 2H), 1.27 (s, 36H). ^{13}C NMR (101 MHz, $CDCl_3$) δ 150.85, 143.05, 140.83, 139.93, 139.50, 137.84, 137.71, 132.09, 128.47, 128.35, 127.21, 126.67, 126.34, 125.08, 124.05, 123.63, 122.42, 120.63, 119.81, 115.57, 110.32, 109.59, 34.44, 31.81. MALDI-TOF-MS (m/z) of $C_{83}H_{73}N_5$ for [M]+: calcd. 1140.095; found, 1140.532.

Synthesis of (2r,3s,5s,6s)-3,5-di(9H-carbazol-9-yl)-2,6-bis(3,6-di-tert-butyl-9H-carbazol-9-yl)-5'-phenyl-[1,1':3',1''-terphenyl]-4-carbonitrile (HCB-3).

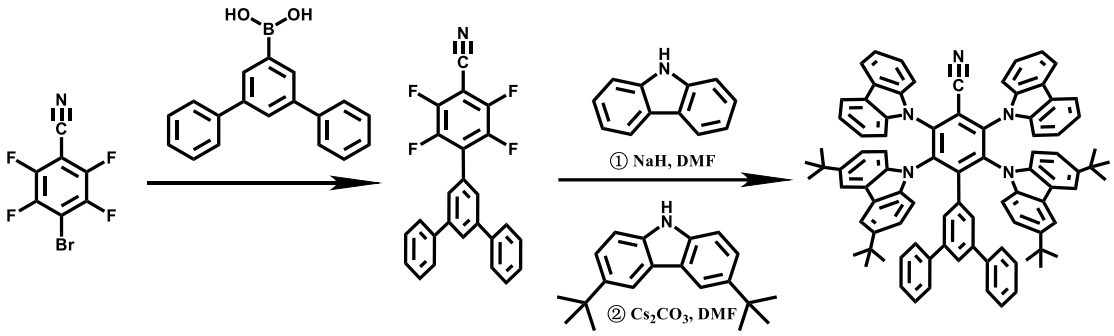

Scheme S3. Synthesis of HCB-3.

Step (1): Compound 4-bromo-2,3,5,6-tetrafluorobenzonitrile (1.0 g, 3.9 mmol) and [1,1':3',1''-terphenyl]-5'-ylboronic acid (1.28 g, 4.7 mmol) were dissolved in 40 mL 1,4-Dioxane. Then $Pd[P(Ph)_3]_4$ (5% equi) and K_3CO_3 (1.1 g, 7.9 mmol) dissolved in water

(3.7 ml) were added in a nitrogen atmosphere. After the solution was heated at 105 °C for 18 hours, the reaction mixture was cooled to room temperature. The crude product was further purified by column chromatography on silica gel (DCM: hexane=1:4) to give 1.23 g (yield: 74%) of 2,3,5,6-tetrafluoro-5'-phenyl-[1,1':3',1''-terphenyl]-4-carbonitrile compound with methane (1:1) as a white powder.

Step (2): Carbazole (1.1 g, 6.4 mmol) and NaH (0.26 g, 11.0 mmol) were stirred for 30 min in N, N- Dimethylformamide (25 mL) in three-neck bottle under nitrogen at 0 ℃ .Then compound 2,3,5,6-tetrafluoro-5'-phenyl-[1,1':3',1''-terphenyl]-4-carbonitrile compound with methane (1:1) (1.1 g 2.6 mmol) which dissolved in 35 mL dry N, N-Dimethylformamide was injected into the bottle and the reaction mixture was stirred 24 h at room temperature. Then, 3,6-di-tert-butyl-9H-carbazole (1.44 g, 5.1 mmol), Cs_2CO_3 (2.2 g, 6.8 mmol) and dry N, N-Dimethylformamide (30 ml) were added into the mixture. After the reaction mixture was stirred under N_2 atmosphere at 150 °C for 24 h. The mixture solution was poured into 250 mL water, and the green precipitates was collected by filtration under a reduced pressure. The crude product was further purified by column chromatography on silica gel (DCM: hexane=1:4) to give 0.93 g (yield: 47%) of **(2r,3s,5s,6s)-3,5-di(9H-carbazol-9-yl)-2,6-bis(3,6-di-tert-butyl-9H-carbazol-9-yl)-5'-phenyl-[1,1':3',1''-terphenyl]-4-carbonitrile** as a green powder. ^{1}H NMR (400 MHz, $CDCl_3$) δ 7.75 (dd, J = 7.0, 1.6 Hz, 4H), 7.57 (d, J = 1.8 Hz, 4H), 7.30 (d, J = 7.7 Hz, 4H), 7.18 – 7.08 (m, 10H), 6.99 (dt, J = 19.2, 8.2 Hz, 12H), 6.83 (dd, J = 6.8, 1.6 Hz, 3H), 6.36 – 6.27 (m, 4H), 1.30 (s, 36H). ^{13}C NMR (101 MHz, $CDCl_3$) δ 151.70, 143.05, 141.73, 140.76, 140.34, 139.96, 138.09, 137.84, 133.18, 128.22, 126.92, 126.82, 125.69, 125.43, 124.24, 123.44, 122.79, 120.85, 120.03, 115.60, 110.30, 109.65, 34.48, 31.8. MALDI-TOF-MS (m/z) of $C_{89}H_{77}N_5$ for [M]+: calcd. 1216.578; found, 1216.630.

^{1}H and ^{13}C NMR of the products

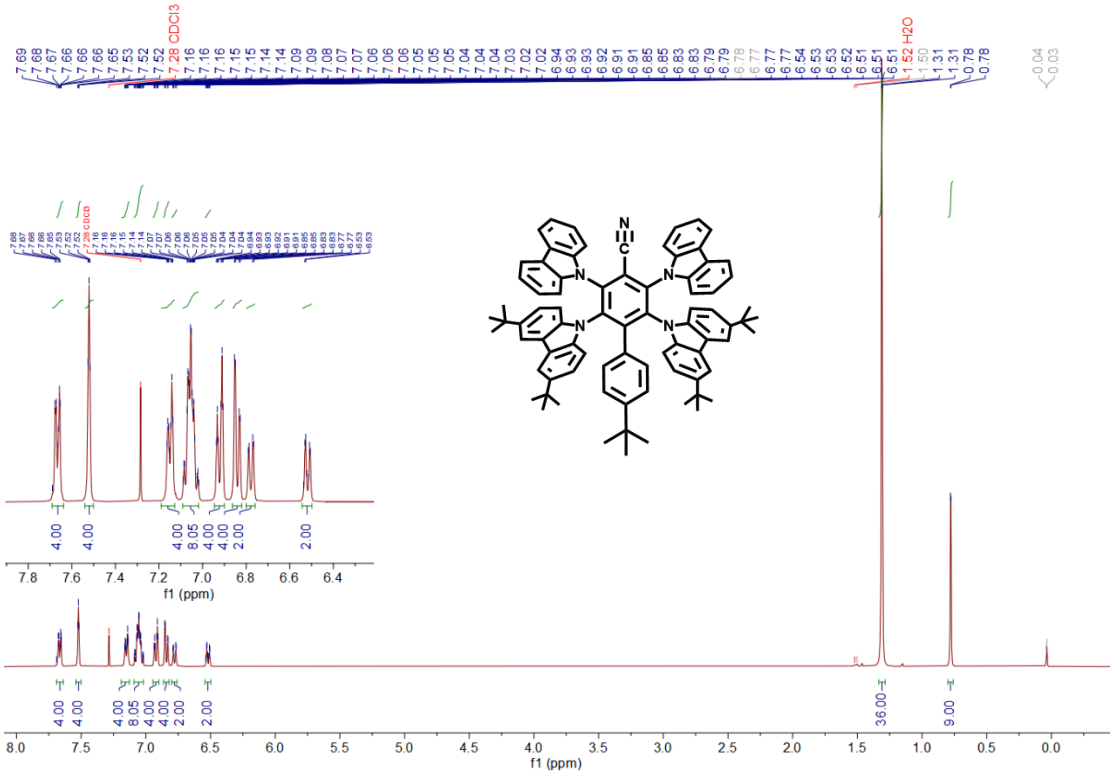

Fig. S1 ^{1}H NMR spectrum of HCB-1.

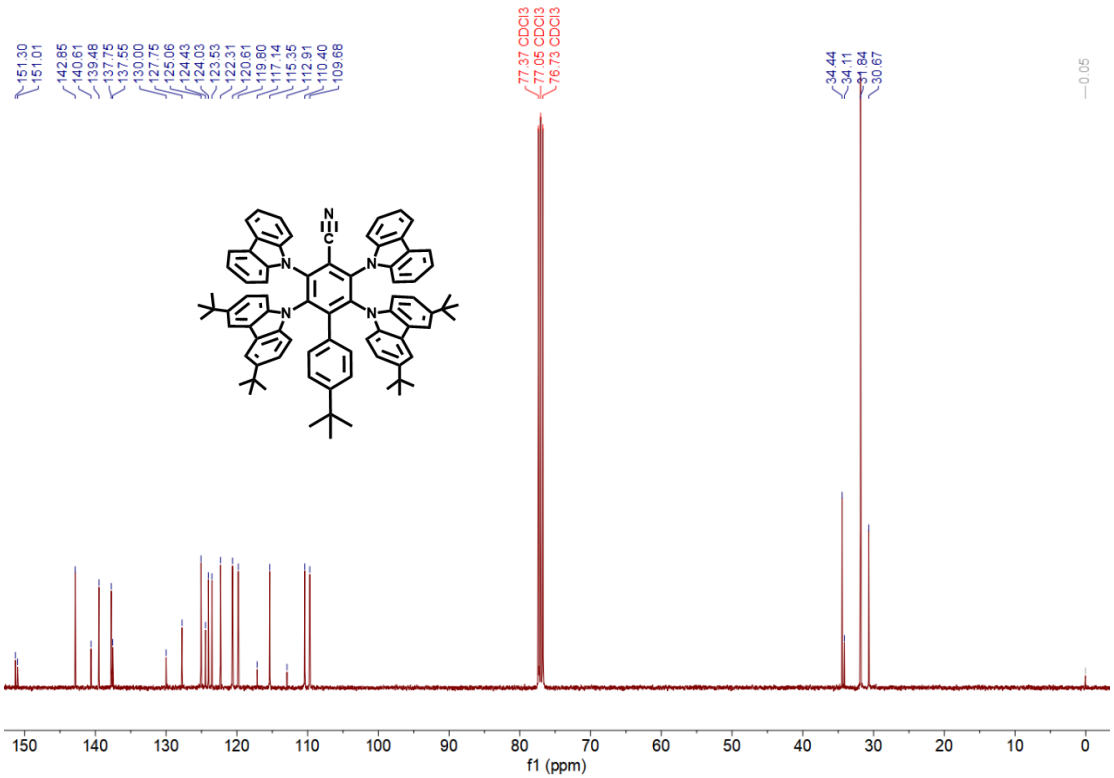

Fig. S2 ^{13}C NMR spectrum of HCB-1.

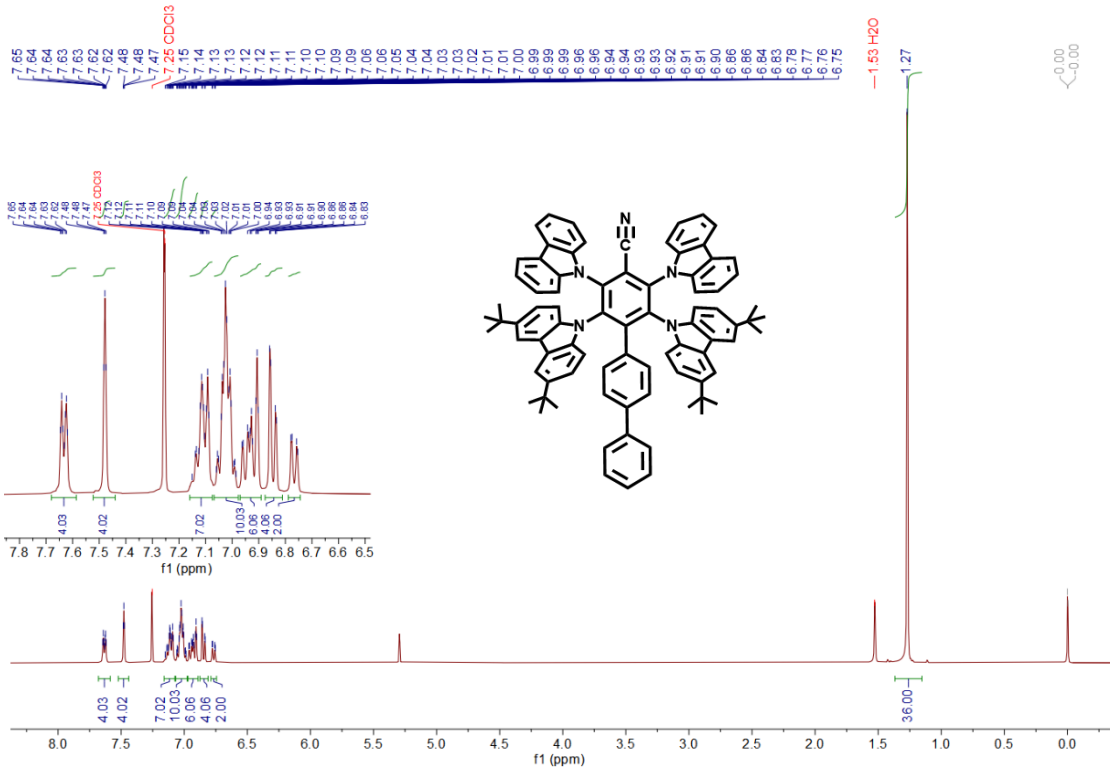

Fig. S3 ^{1}H NMR spectrum of HCB-2.

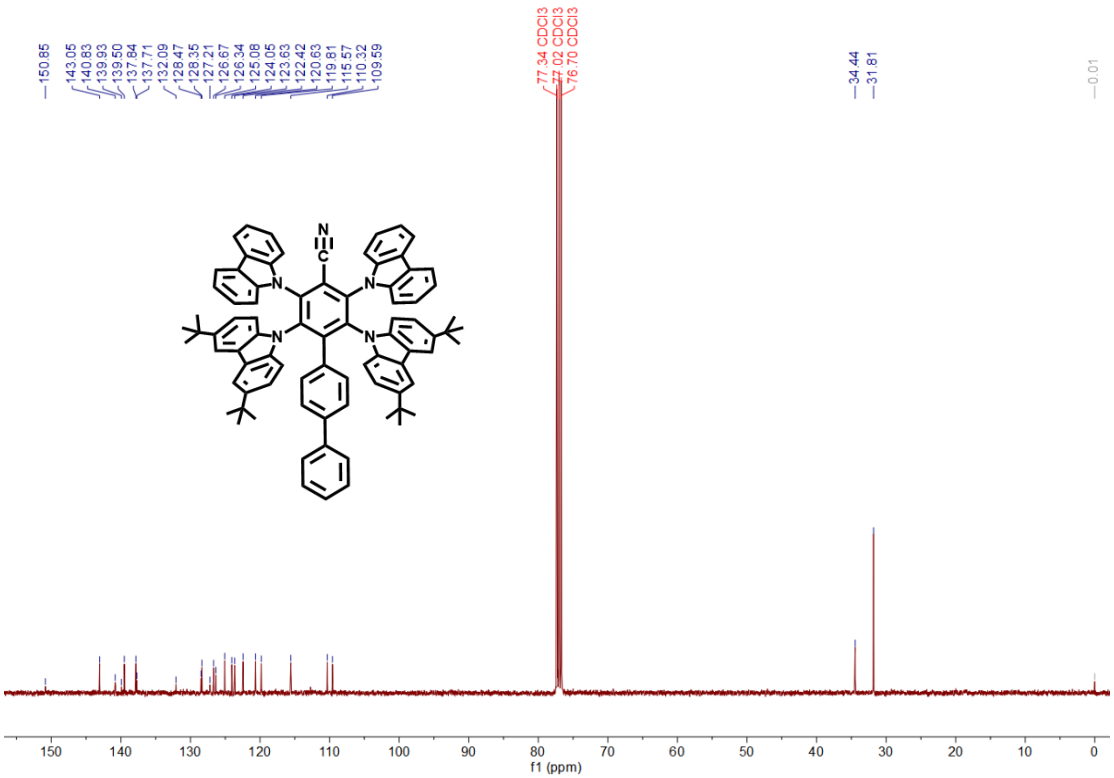

Fig. S4 ^{13}C NMR spectrum of HCB-2.

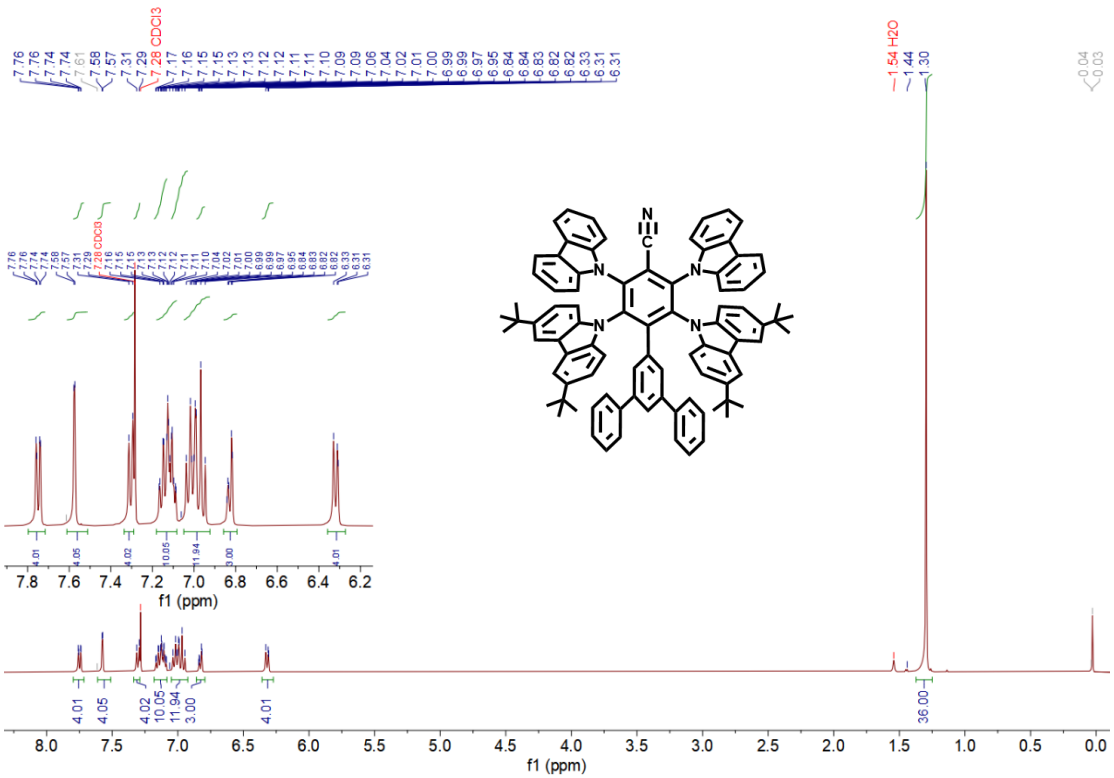

Fig. S5 ^{1}H NMR spectrum of HCB-3.

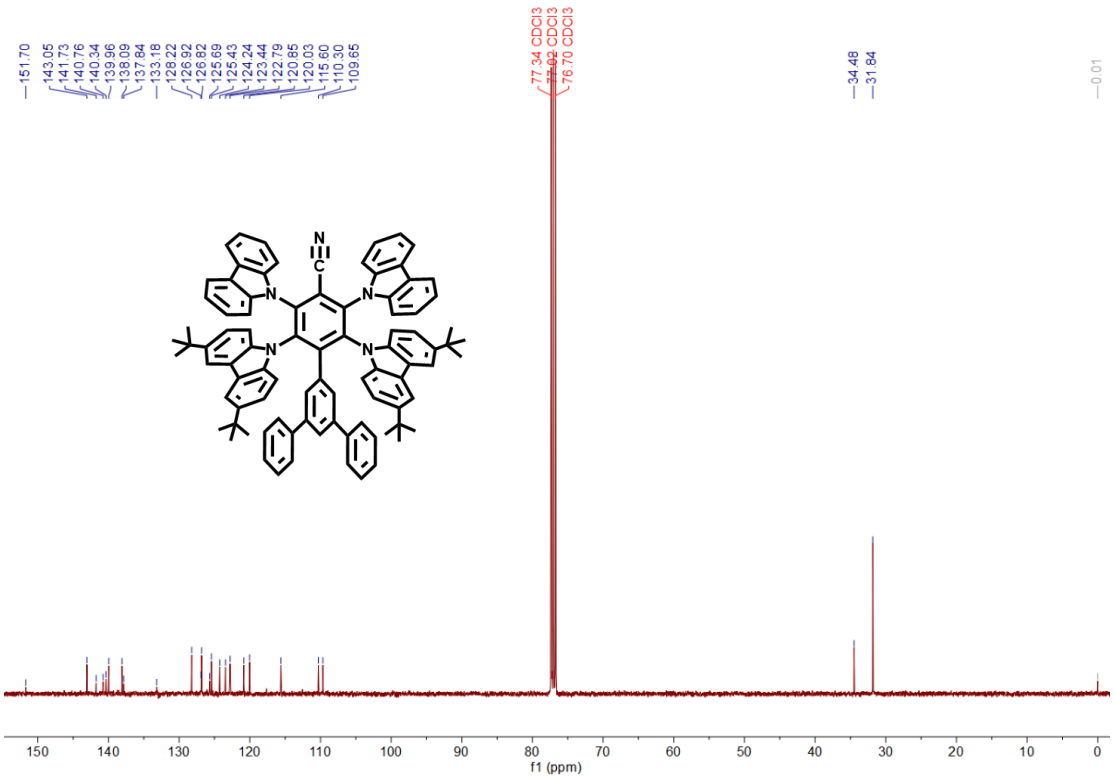

Fig. S6 ^{13}C NMR spectrum of HCB-3.

MALDI-TOF of the products

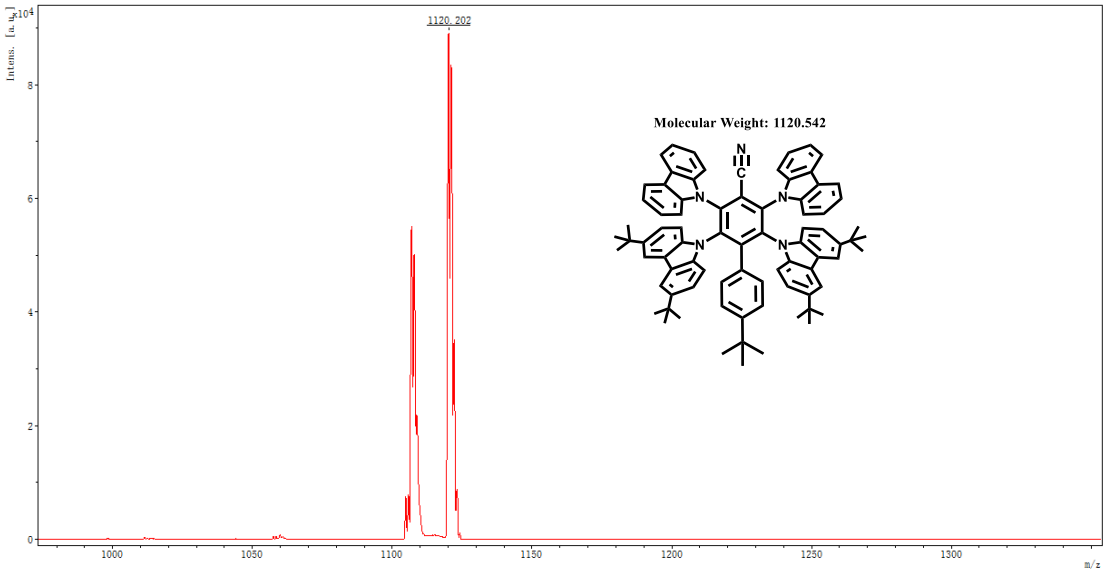

Fig. S7 TOF-MS spectrum of HCB-1.

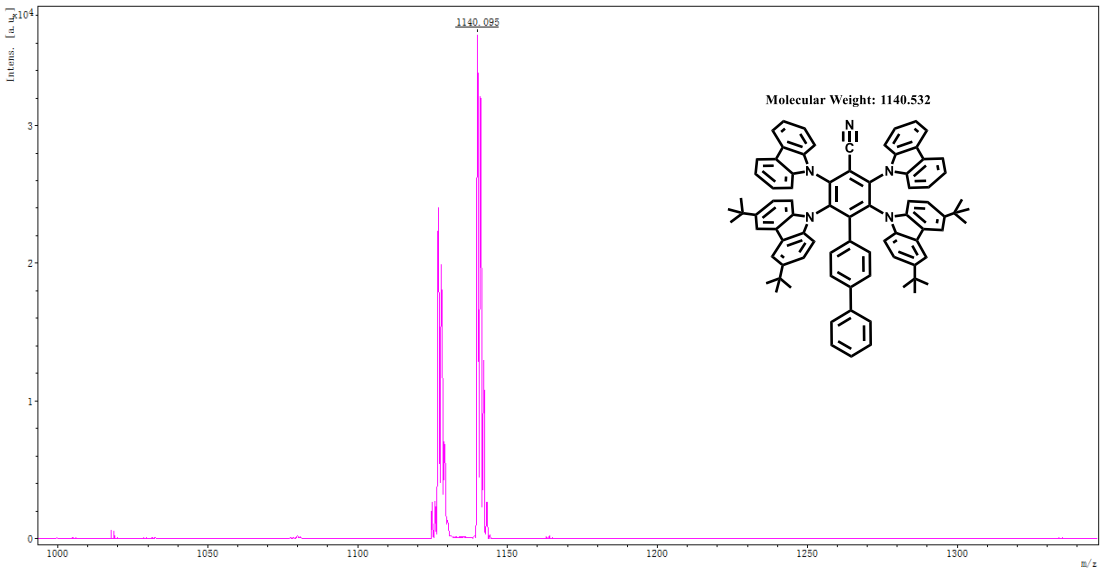

Fig. S8 TOF-MS spectrum of HCB-2.

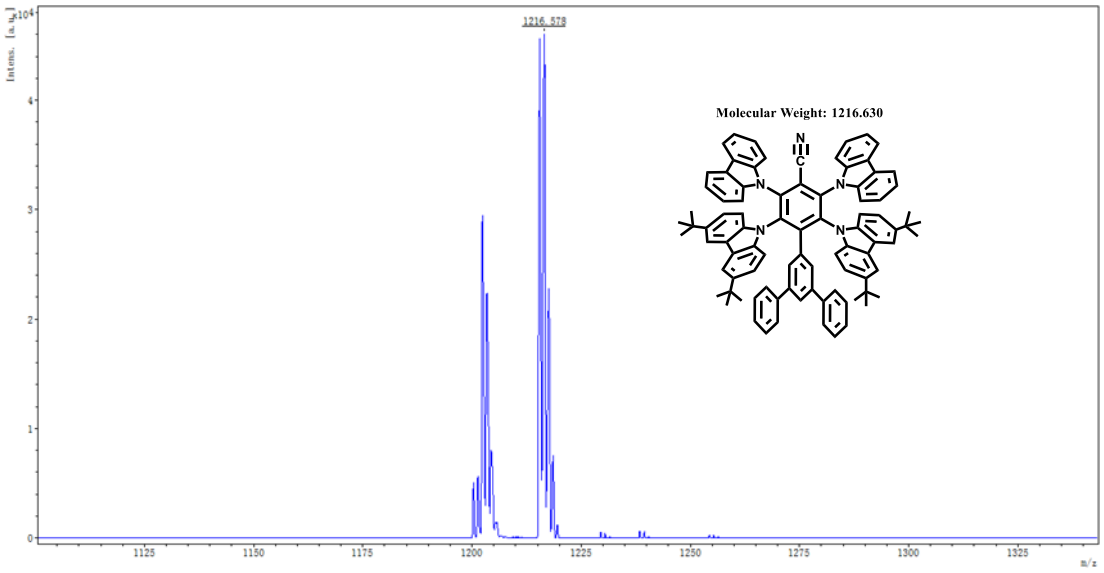

Fig. S9 TOF-MS spectrum of HCB-3.

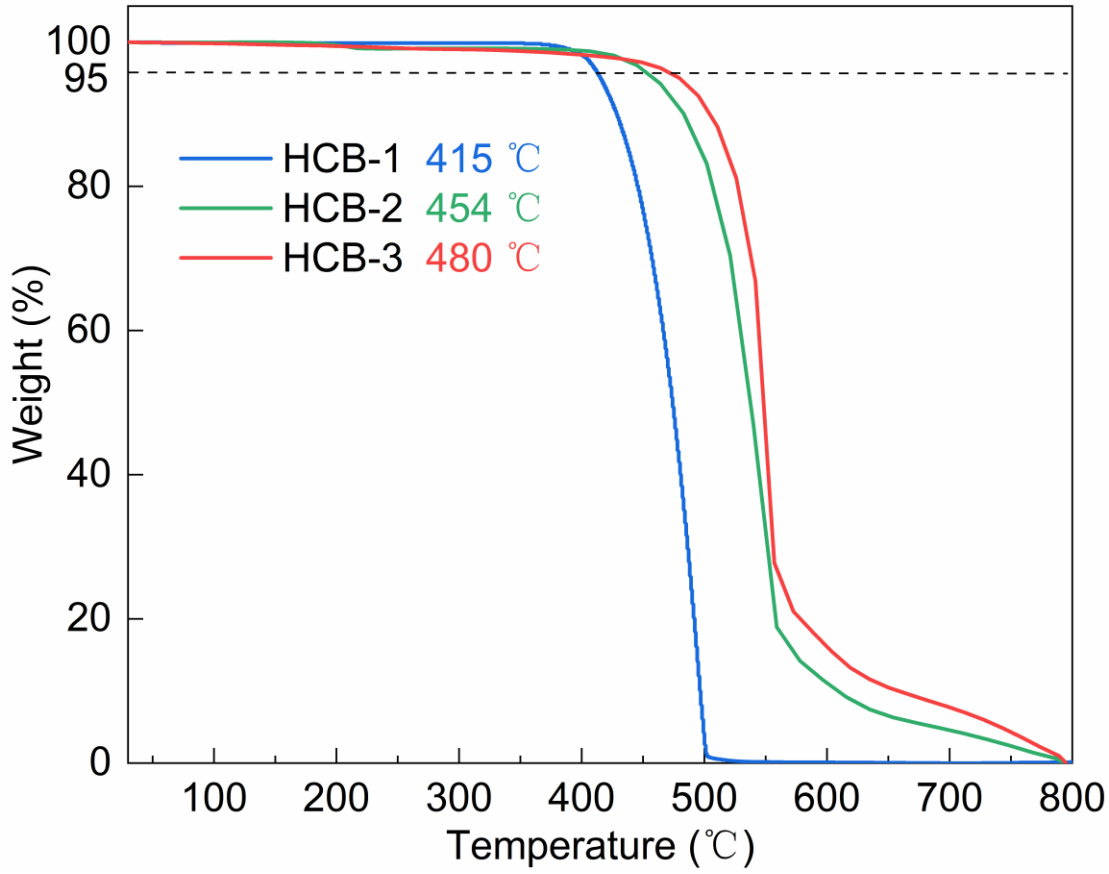

Fig. S10 TGA curves of HCB-1, HCB-2, and HCB-3.

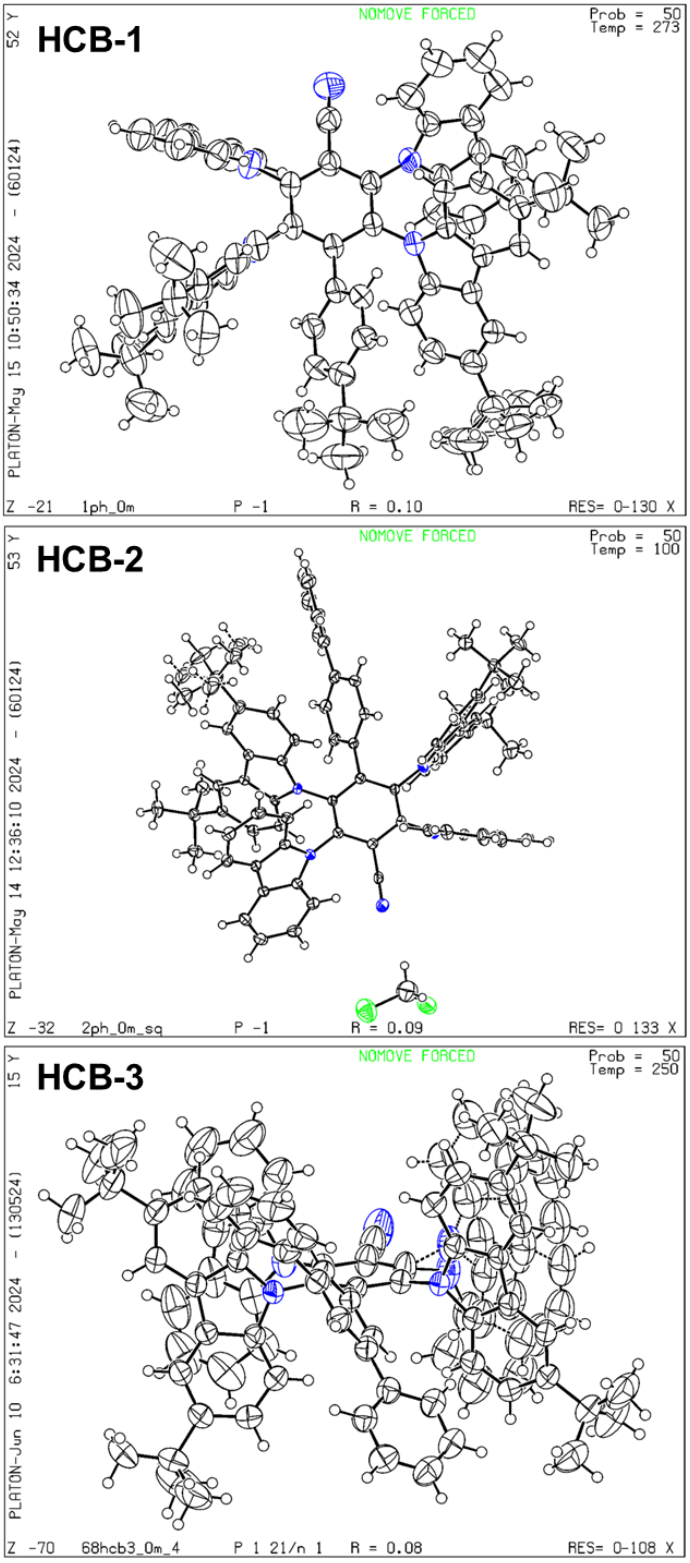

Fig. S11 Ellipsoid plot of HCB-1, HCB-2, and HCB-3 obtained by single crystal diffraction.

Table S1. Crystal data and structure refinement for HCB-1.

Compound	HCB-1
Empirical formula	$C_{81}H_{77}N_5$
CCDC number	2364901
Temperature/K	273
Crystal system	triclinic
Space group	P-1
a/Å	11.898(4)
b/Å	13.679(5)
c/Å	22.573(8)
α/°	73.668(11)
β/°	79.199(10)
γ/°	71.603(11)
Volume/Å^3	3326(2)
Z	2
ρ_{calc}g/cm^3	1.119
μ/mm^{-1}	0.065
F(000)	1196
Crystal size/mm^3	0.15 × 0.08 × 0.05
Radiation	MoKα (λ = 0.71073)
2Θ range for data collection/°	3.782 to 52.844
Index ranges	$-14 \le h \le 14$, $-16 \le k \le 17$, $-28 \le l \le 28$
Reflections collected	36017
Independent reflections	13353 [R_{int} = 0.0759, R_{sigma} = 0.1062]
Data/restraints/parameters	13353/1770/820
Goodness-of-fit on F^2	1.174
Final R indexes [I>=2σ (I)]	R_1 = 0.0961, wR_2 = 0.2262
Final R indexes [all data]	R_1 = 0.2013, wR_2 = 0.2804
Largest diff. peak/hole / e Å^{-3}	0.65/-0.49

Table S2. Crystal data and structure refinement for HCB-2.

Compound	HCB-2
Empirical formula	$C_{84}H_{75}Cl_2N_5$
CCDC number	2364902
Temperature/K	100
Crystal system	triclinic
Space group	P-1
a/Å	11.9195(2)
b/Å	14.7278(3)
c/Å	21.6227(4)
α/°	84.2410(10)
β/°	78.2020(10)
γ/°	69.5210(10)
Volume/Å^3	3479.09(11)
Z	2
ρ_{calc}g/cm^3	1.17
μ/mm^{-1}	1.204
F(000)	1296
Crystal size/mm^3	0.15 × 0.08 × 0.05
Radiation	CuKα (λ = 1.54178)
2Θ range for data collection/°	4.176 to 127.83
Index ranges	-13 ≤ h ≤ 13, -17 ≤ k ≤ 17, -25 ≤ l ≤ 24
Reflections collected	22352
Independent reflections	11303 [R_{int} = 0.0606, R_{sigma} = 0.0765]
Data/restraints/parameters	11303/971/862
Goodness-of-fit on F^2	1.045
Final R indexes [I>=2σ (I)]	R_1 = 0.0867, wR_2 = 0.2242
Final R indexes [all data]	R_1 = 0.1025, wR_2 = 0.2406
Largest diff. peak/hole / e Å^{-3}	1.18/-1.37

Table S3 Crystal data and structure refinement for HCB-3.

Compound	HCB-3
Empirical formula	$C_{89}H_{77}N_5$
CCDC number	2364903
Temperature/K	250
Crystal system	monoclinic
Space group	P21/n
a/Å	11.6574(4)
b/Å	21.0626(7)
c/Å	30.0359(9)
α/°	90
β/°	94.411(2)
γ/°	90
Volume/Å^3	7353.0(4)
Z	4
ρ_{calc}g/cm^3	1.099
μ/mm^{-1}	0.485
F(000)	2584
Crystal size/mm^3	0.15 × 0.09 × 0.08
Radiation	CuKα (λ = 1.54178)
2Θ range for data collection/°	5.13 to 127.844
Index ranges	$-13 \le h \le 13$, $0 \le k \le 24$, $0 \le l \le 34$
Reflections collected	11809
Independent reflections	11809 [R_{int} = ?, R_{sigma} = 0.0753]
Data/restraints/parameters	11809/1341/969
Goodness-of-fit on F^2	1.056
Final R indexes [I>=2σ (I)]	R_1 = 0.0808, wR_2 = 0.2241
Final R indexes [all data]	R_1 = 0.1146, wR_2 = 0.2690
Largest diff. peak/hole / e Å^{-3}	0.42/-0.26

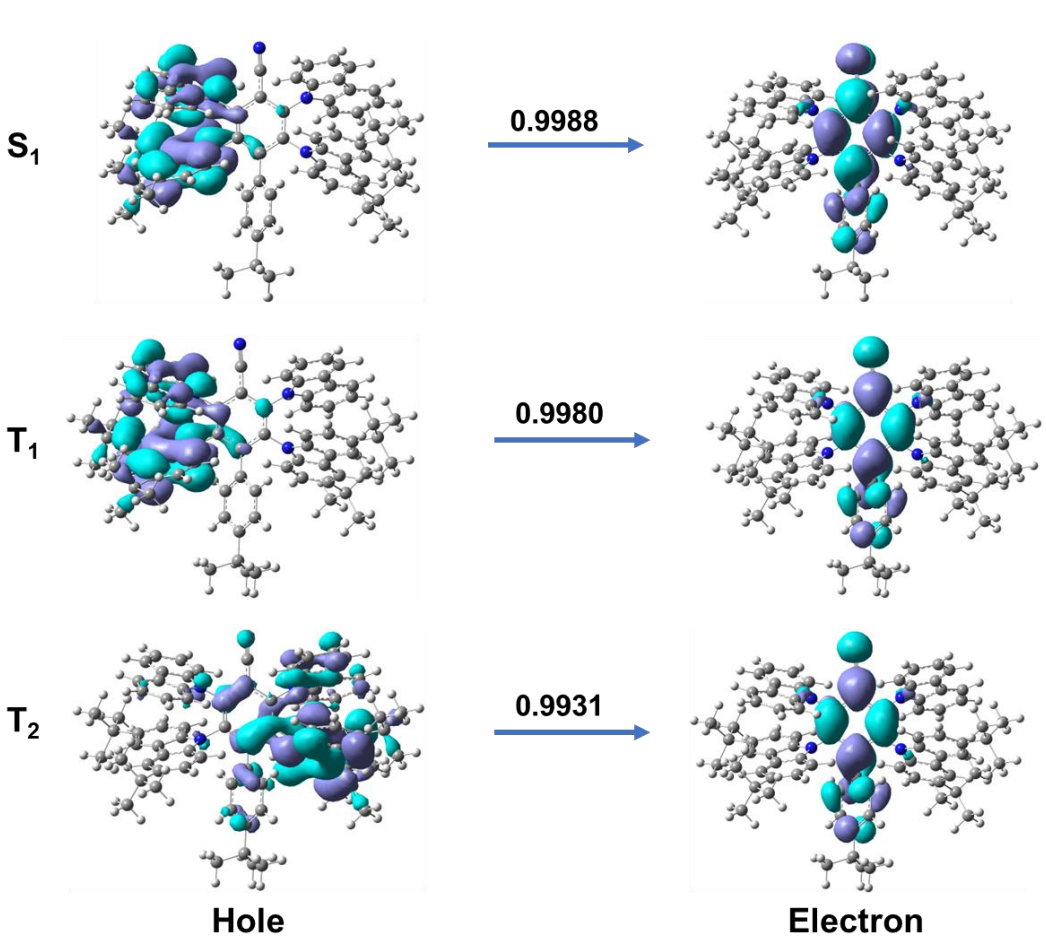

Fig. S12 The NTO diagram of HCB-1.

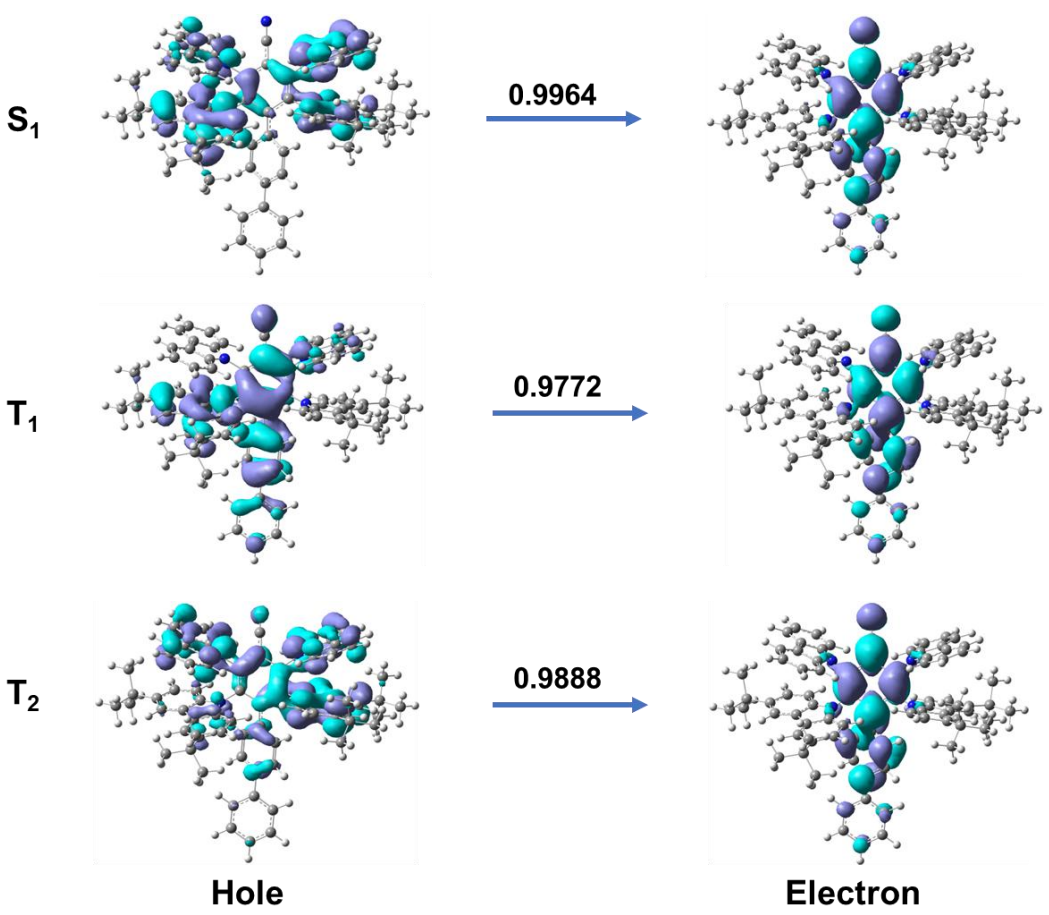

Fig. S13 The NTO diagram of HCB-2.

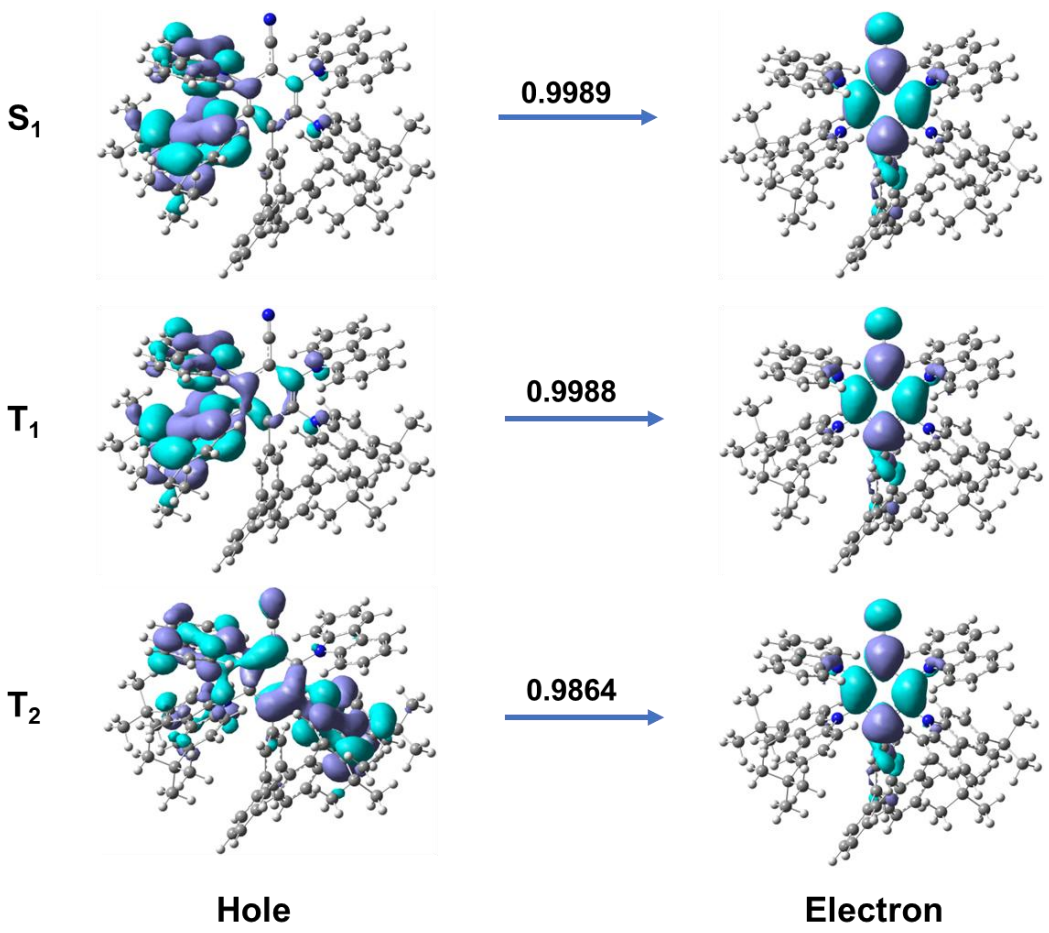

Fig. S14 The NTO diagram of HCB-3.

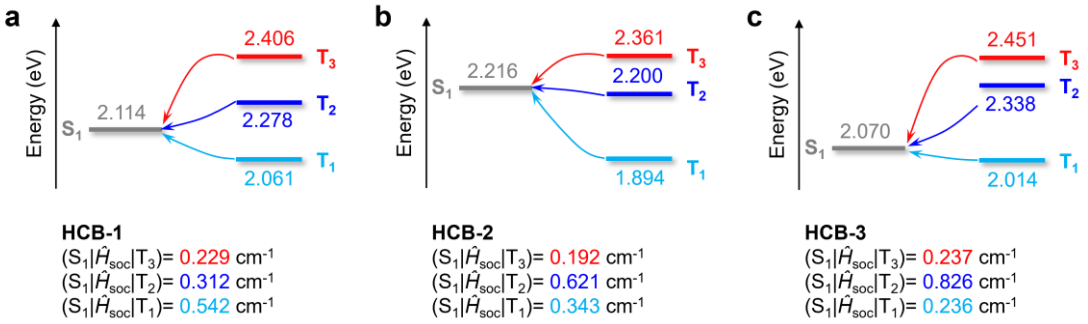

Fig. S15 The calculated energies and SOC constants between S_1 and $T_{1\text{-}3}$ states for all TADF emitters.

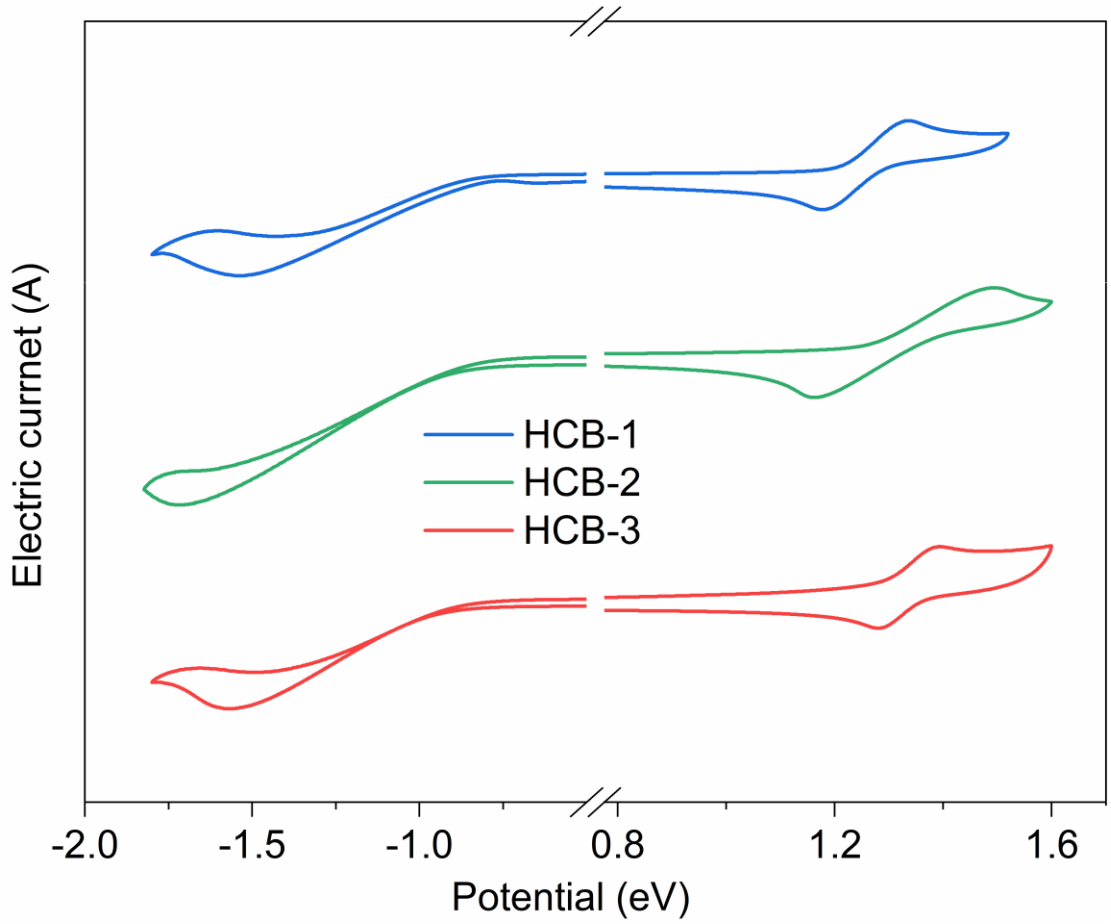

Fig. S16 CV diagrams of HCB-1, HCB-2, and HCB-3.

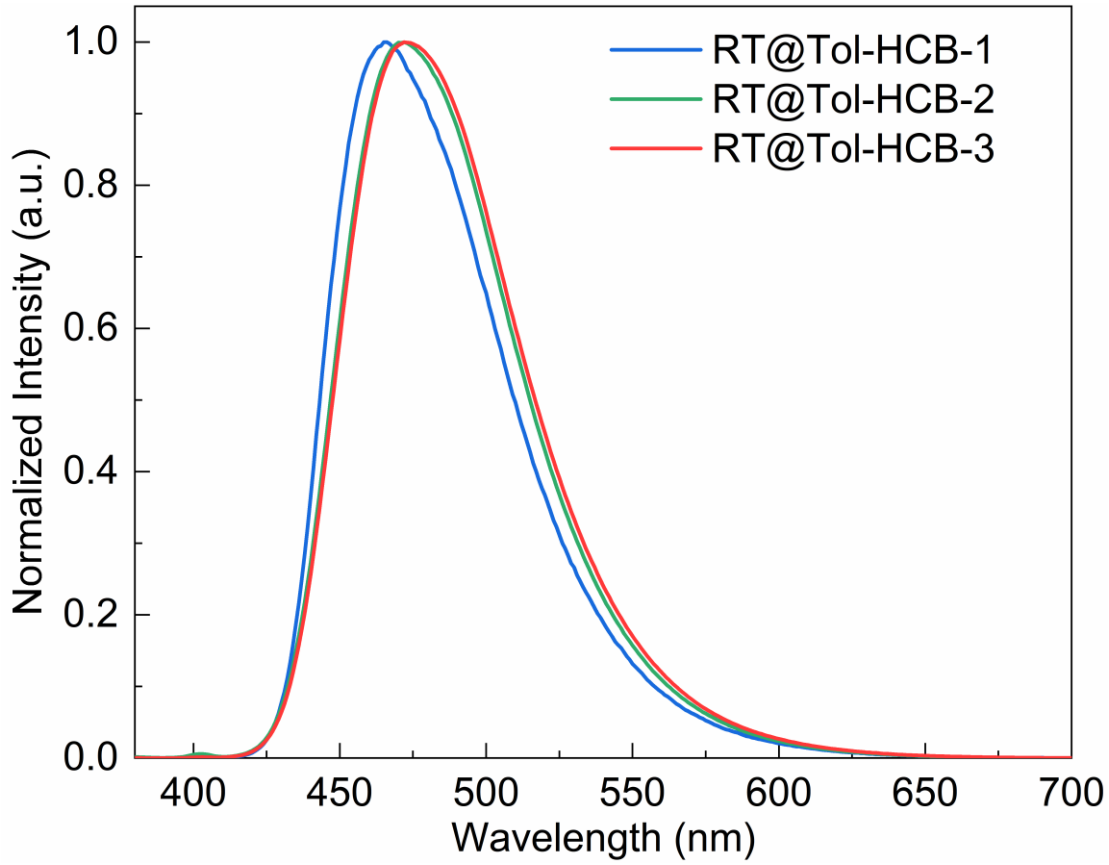

Fig. S17 PL spectra of HCB-1, HCB-2, and HCB-3 measured in toluene at room-temperature (RT).

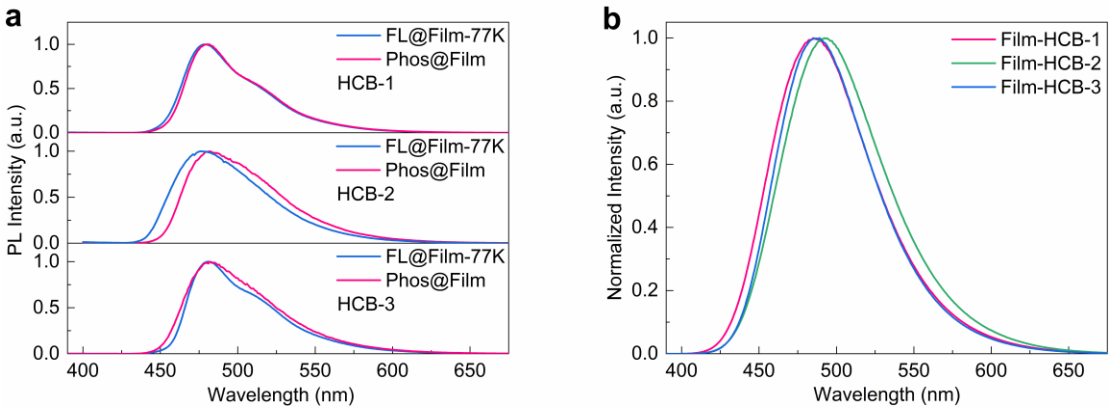

Fig. S18 a) Phosphorescence and PL spectra of HCB-1, HCB-2, and HCB-3 measured in pure film at 77 K. b) PL spectra of HCB-1, HCB-2, and HCB-3 measured in 100 wt% film at RT.

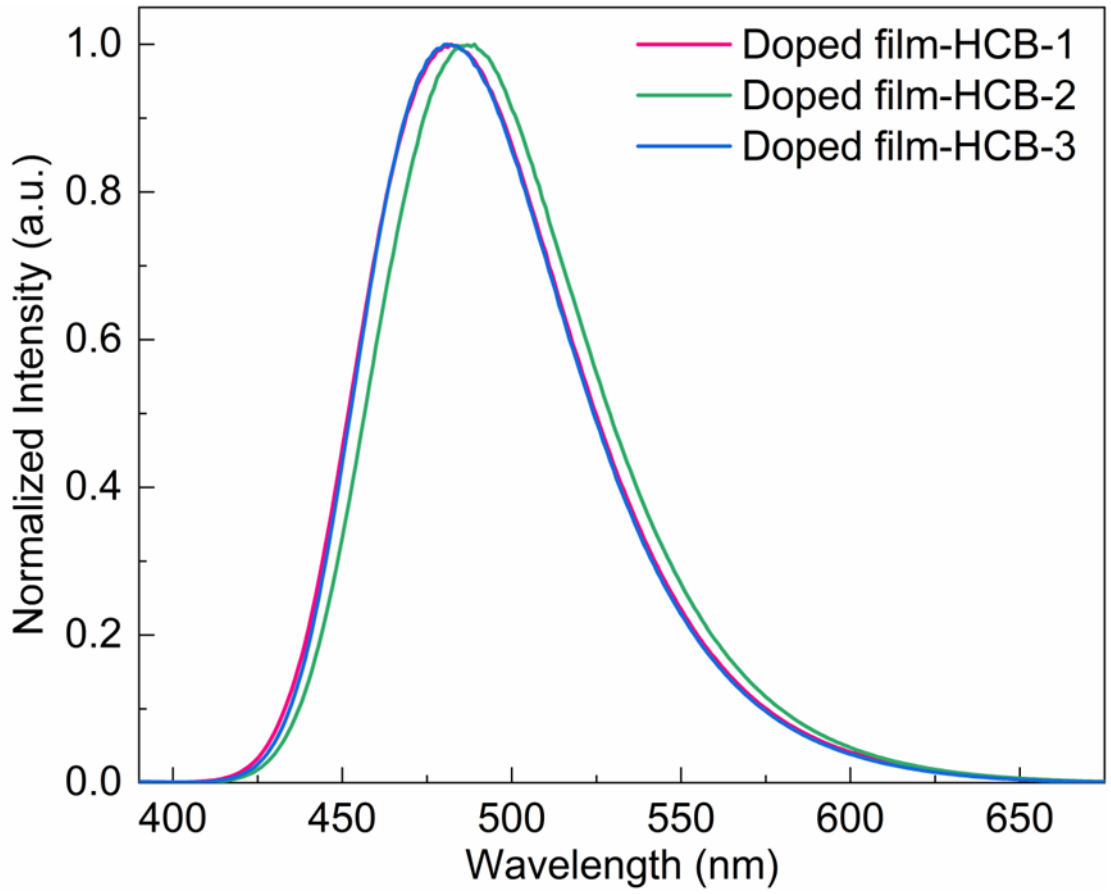

Fig. S19 PL spectra of HCB-1, HCB-2, and HCB-3 measured in 20 wt% film at room-temperature (RT).

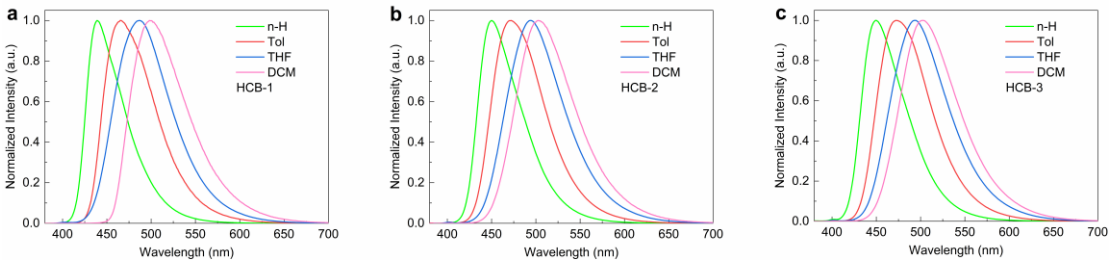

Fig. S20 PL spectra of a) HCB-1, b) HCB-2, and c) HCB-3 in various solvents (n-H: n-hexane, Tol: toluene, THF: tetrahydrofuran, DCM: dichloromethane).

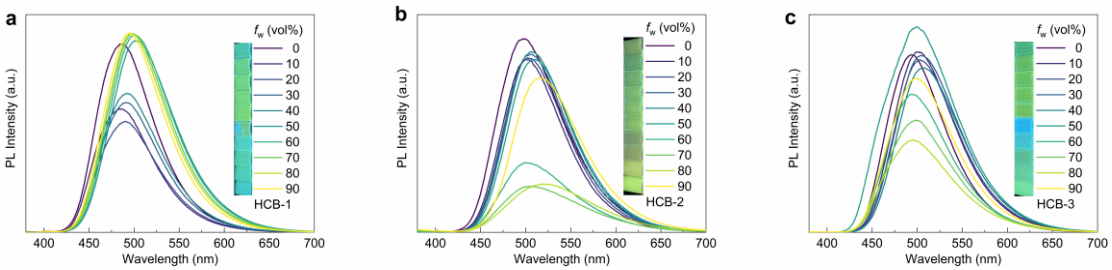

Fig. S21 PL spectra of a) HCB-1, b) HCB-2, and c) HCB-3 in THF/H_2O mixtures with different water fractions (f_w = 0% ~ 90%).

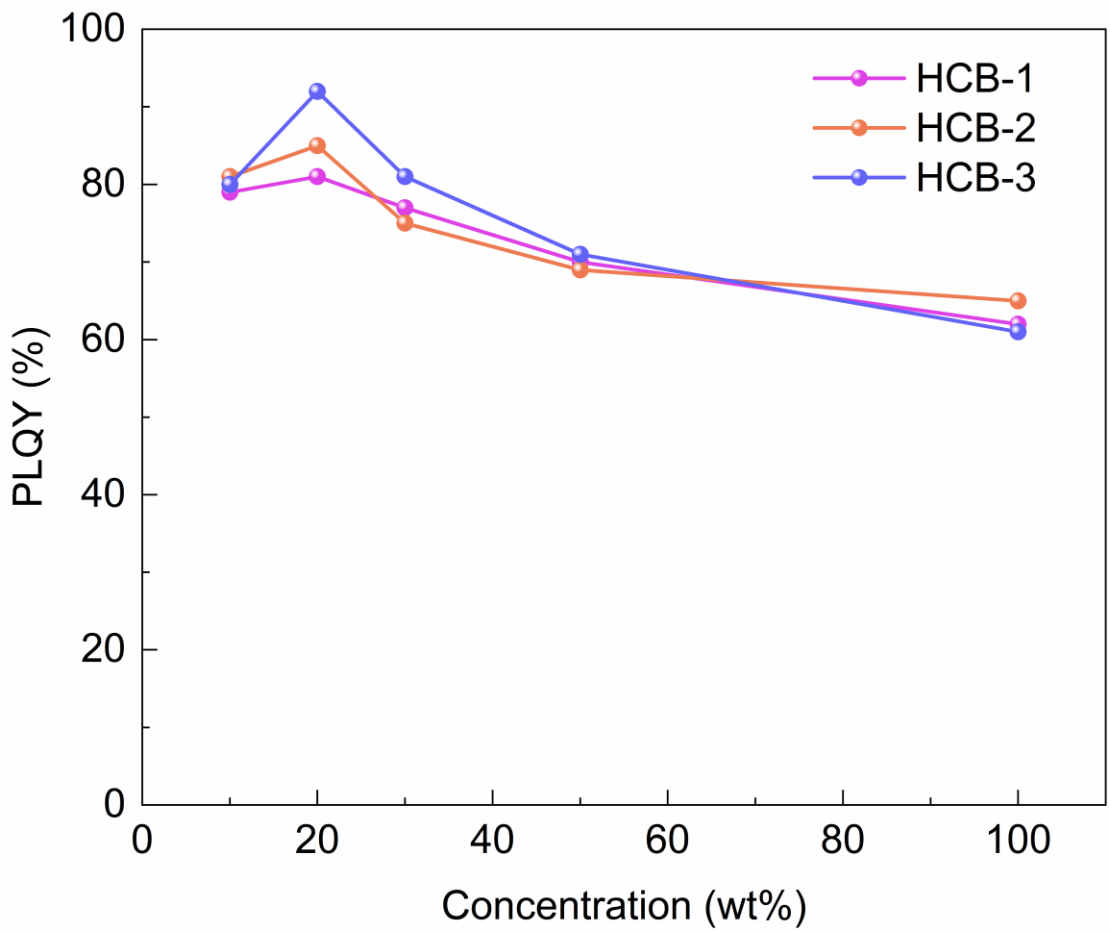

Fig. S22 The doping concentration dependence on PLQY of HCB-1, HCB-2 and HCB-3 in mCP.

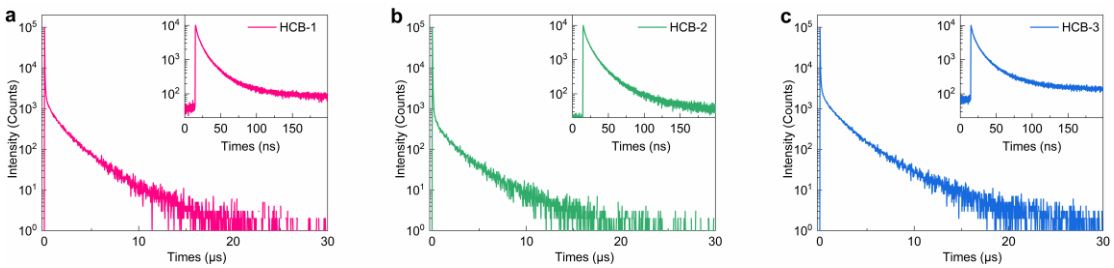

Fig. S23 Transient PL decay curves of a) HCB-1, b) HCB-2, and c) HCB-3 in 100 wt% films.

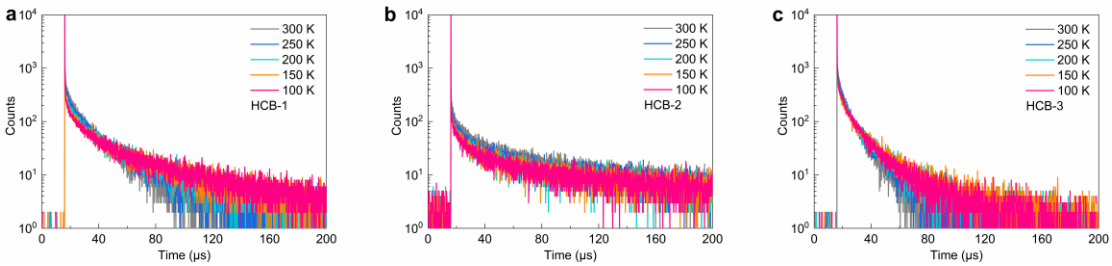

Fig. S24 Temperature-dependent TRPL of a) HCB-1, b) HCB-2, and c) HCB-3 in doped films.

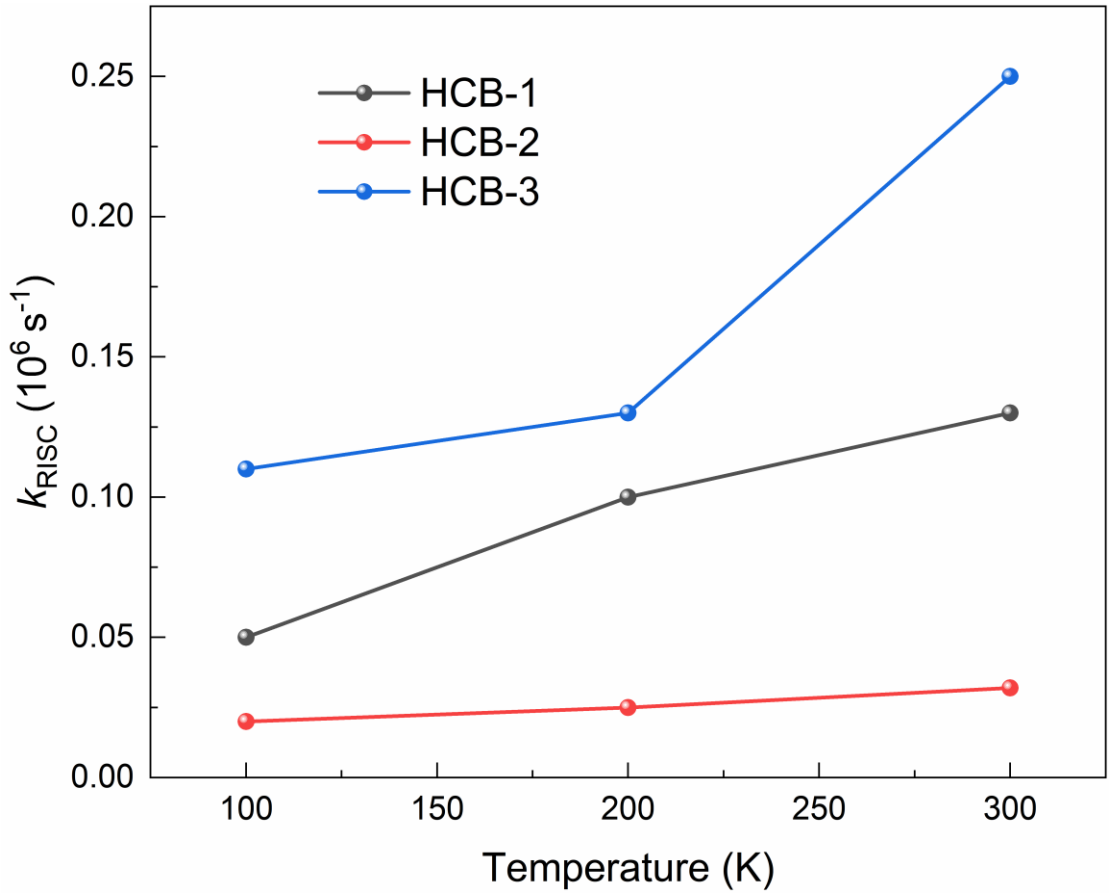

Fig. S25 Temperature-dependent TRPL of a) HCB-1, b) HCB-2, and c) HCB-3 in doped films.

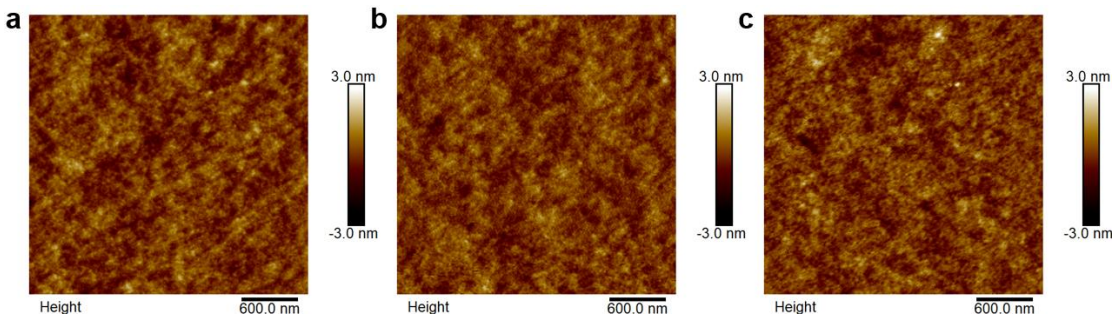

Fig. S26 AFM images of 20 wt% doped films. a) HCB-1 (RMS=0.373 nm), b) HCB-2 (RMS=0.349 nm), c) HCB-3 (RMS=0.376 nm). (Solution-processed films structure: ITO/PEDOT: PSS/PVK/mCP: TADF emitter)

Table S4 Photophysical characteristics of HCB-1, HCB-2, and HCB-3.

Films[a]	Φ_p [%][b]	Φ_d [%][b]	τ_p [ns][c]	τ_d [μs][c]	k_r [10^6 s^{-1}][d]	k_{nr} [10^6 s^{-1}][e]	k_{ISC} [10^6 s^{-1}][f]	k_{RISC} [10^6 s^{-1}][g]
HCB-1	43	38	35.24	15.23	12.10	2.84	13.44	0.13
HCB-2	61	24	29.43	57.83	20.58	3.63	9.77	0.03
HCB-3	42	50	41.43	8.71	10.15	0.88	13.11	0.25

[a] 20 wt% HCB-1, 20 wt% HCB-2 and 20 wt% HCB-3 doped in mCP film.

[b] Quantum yields for prompt fluorescence (Φ_p) and delayed fluorescence (Φ_d) for the neat film, $\Phi_p + \Phi_d = \Phi_{PL}$.

[c] Lifetime of the prompt component (τ_p) and delayed component (τ_d) as determined from the transient PL.

[d] Radiative rate constants of S_1, $k_r = \Phi_p/\tau_p + \Phi_d/\tau_d$.

[e] Nonradiative rate constants of S_1, $k_{nr} = k_r(1 - \Phi_{PL})/\Phi_{PL}$.

[f] Rate constants for ISC ($S_1 \rightarrow T_1$), $k_{ISC} = k_p - k_r - k_{nr}$.

[g] Rate constants for RISC ($T_1 \rightarrow S_1$), $k_{RISC} = k_p k_d / k_{ISC} \cdot \Phi_d/\Phi_p$.

Table S5 Photophysical characteristics of HCB-1, HCB-2, and HCB-3 in 100 wt% films.

Films[a]	Φ_p [%][b]	Φ_d [%][b]	τ_p [ns][c]	τ_d [μs][c]	k_r [10^7 s^{-1}][d]	k_{nr} [10^6 s^{-1}][e]	k_{ISC} [10^6 s^{-1}][f]	k_{RISC} [10^6 s^{-1}][g]
HCB-1	56	21	19.47	2.17	2.87	8.59	14.02	0.64
HCB-2	68	12	19.43	2.29	3.51	8.77	7.59	0.52
HCB-3	76	13	20.81	1.93	3.67	4.53	6.84	0.61

[a] HCB-1, HCB-2 and HCB-3 in 100 wt% film.

[b] Quantum yields for prompt fluorescence (Φ_p) and delayed fluorescence (Φ_d) for the neat film, $\Phi_p + \Phi_d = \Phi_{PL}$.

[c] Lifetime of the prompt component (τ_p) and delayed component (τ_d) as determined from the transient PL.

[d] Radiative rate constants of S_1, $k_r = \Phi_p/\tau_p + \Phi_d/\tau_d$.

[e] Nonradiative rate constants of S_1, $k_{nr} = k_r(1 - \Phi_{PL})/\Phi_{PL}$.

[f] Rate constants for ISC ($S_1 \rightarrow T_1$), $k_{ISC} = k_p - k_r - k_{nr}$.

[g] Rate constants for RISC ($T_1 \rightarrow S_1$), $k_{RISC} = k_p k_d / k_{ISC} \cdot \Phi_d/\Phi_p$.

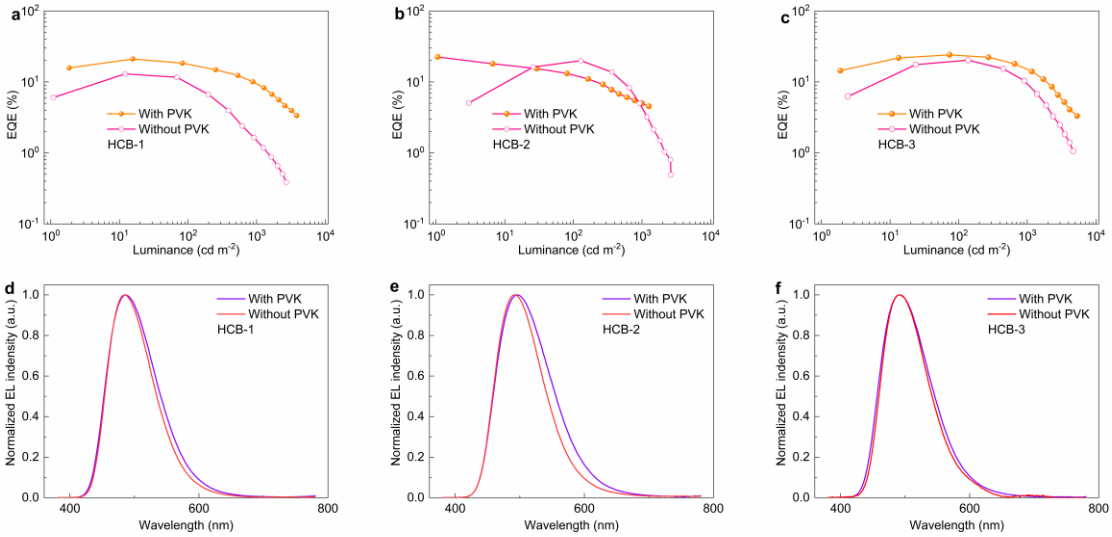

Fig. S27 EL spectra and EQE of HCB-1 (a, d), HCB-2 (b, e) and HCB-3 (c, f) with PVK and without PVK.

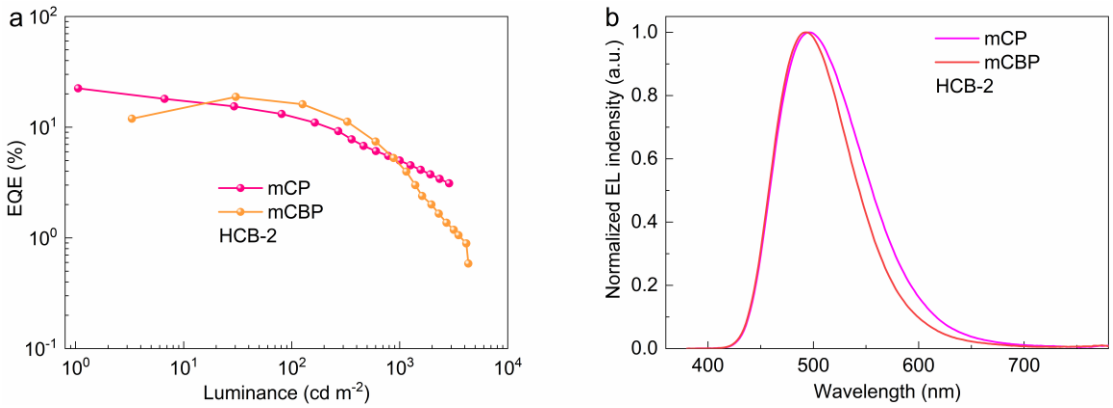

Fig. S28 EL spectra and EQE of HCB-2 (a, b) using mCP and mCBP.

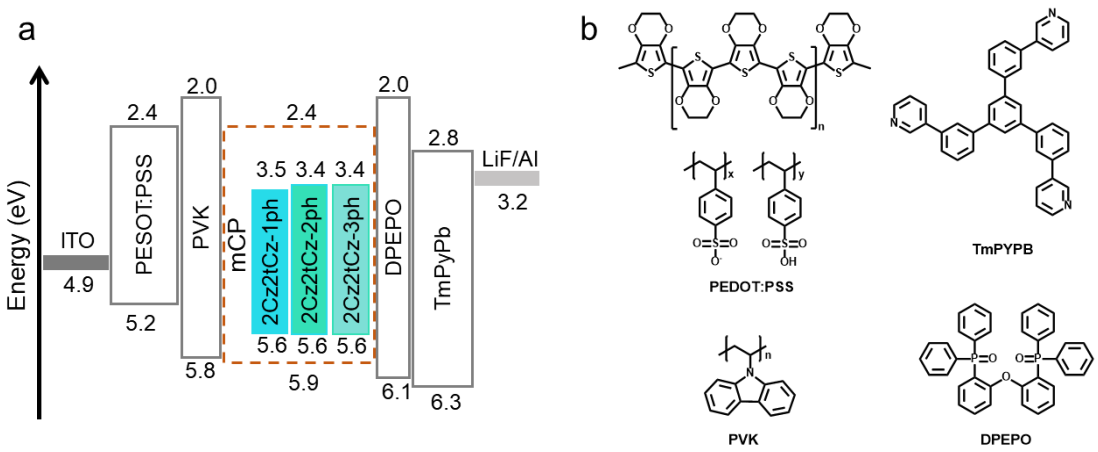

Fig. S29 a) Energy-level diagram. b) Molecular structures employed in the devices.

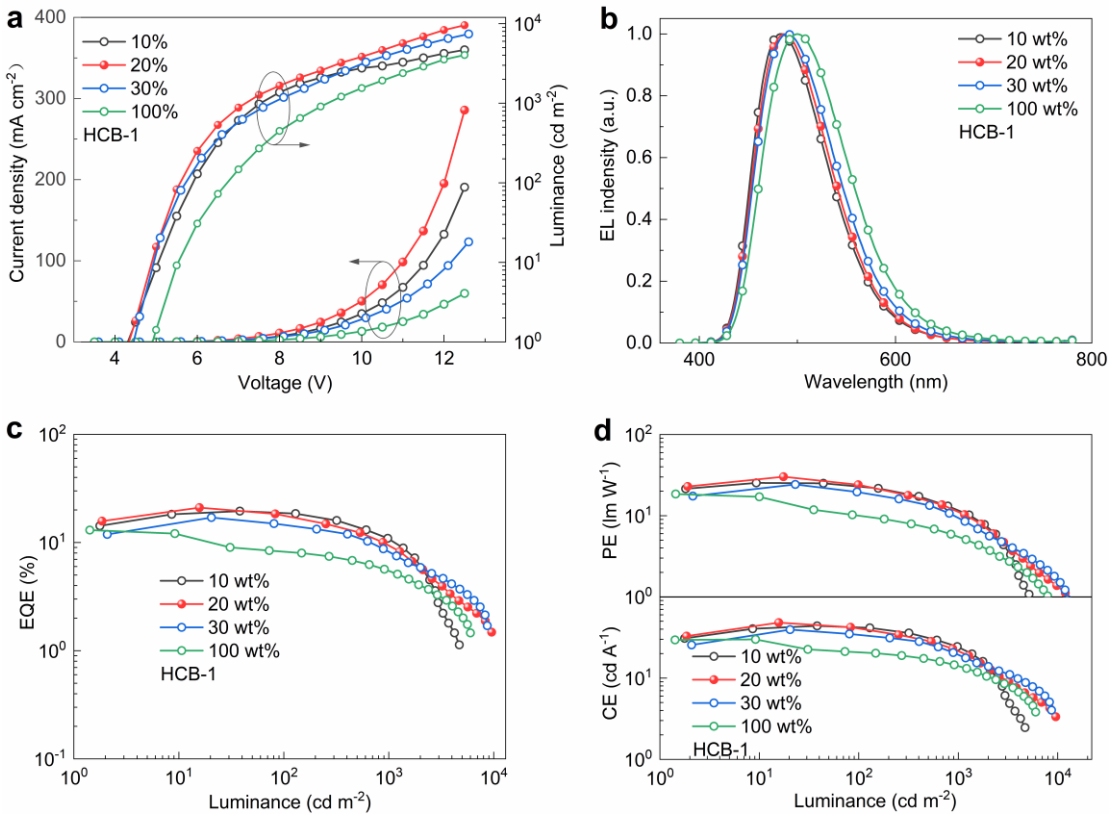

Fig. S30 Device Performance of HCB-1. a) *J-V-L* curves, b) EL spectra. c) EQE as a function of luminance. d) PE and CE as a function of luminance.

Table S6. OLEDs performance based on HCB-1.

EML	V_{on}[a] [V]	EQE[b] [%]	CE[c] [cd A^{-1}]	PE[d] [lm W^{-1}]	λ_{EL}[e] [nm]	FWHM[e] [nm]	CIE[e] (x, y)
HCB-1-10 wt%	4.3	19.5/18.8/11.2	43.8	25.4	484	85	(0.18, 0.35)
HCB-1-20 wt%	4.3	21.0/17.6/9.4	48.1	30.2	486	85	(0.18, 0.36)
HCB-1-30 wt%	4.4	17.0/14.2/8.0	39.4	24.3	488	88	(0.19, 0.37)
HCB-1-100 wt%	4.9	12.1/8.3/5.4	29.9	18.5	500	92	(0.21, 0.39)

[a] Turn-on voltage. [b] Maximum EQE, and values at 100 and 1000 cd/m^2. [c] $EQE_{roll\text{-}off}$ = $(EQE_{max}\text{-}EQE_{100/1000})/EQE_{max}$ [d] Maximum CE and PE. [e] EL peak, FWHM and CIE color coordinates.

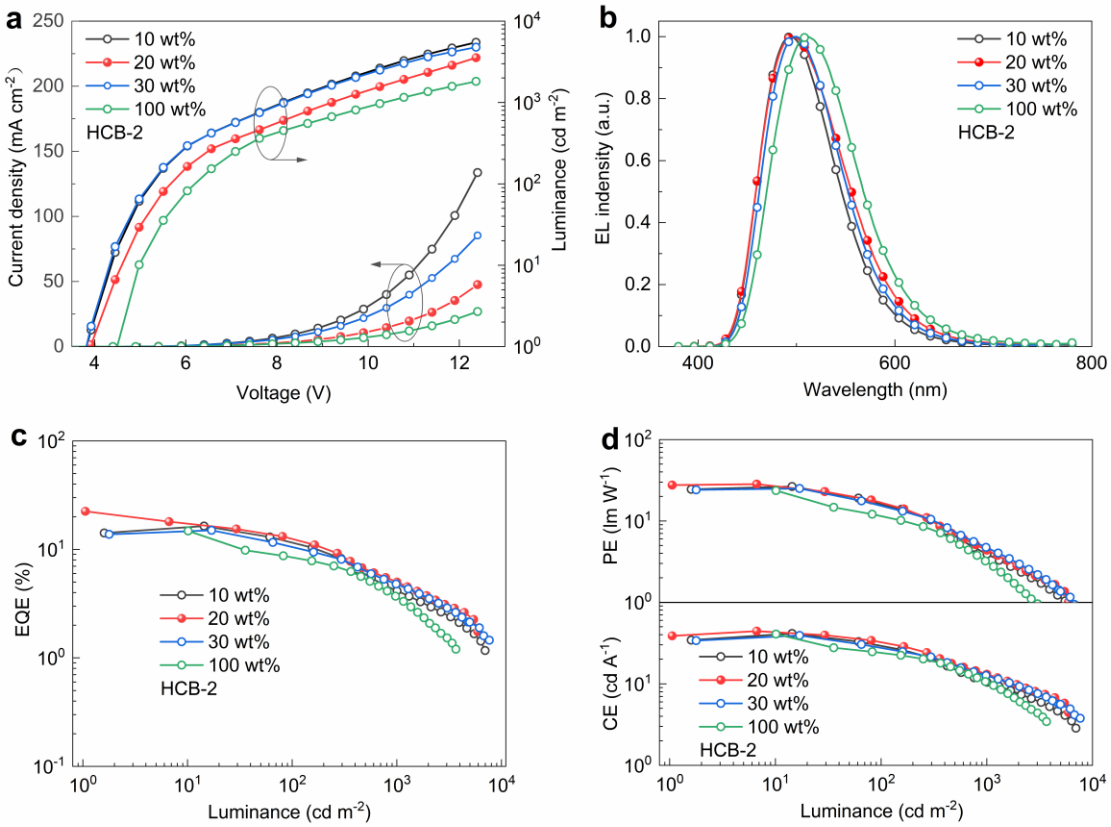

Fig. S31 Device Performance of HCB-2. a) *J-V-L* curves, b) EL spectra. c) EQE as a function of luminance. d) PE and CE as a function of luminance.

Table S7. OLEDs performance based on HCB-2.

EML	V_{on}[a] [V]	EQE[b] [%]	CE[c] [cd A^{-1}]	PE[c] [lm W^{-1}]	λ_{EL}[d] [nm]	FWHM[e] [nm]	CIE[e] (x, y)
HCB-2-10 wt%	4.3	16.4/11.5/4.2	41.3	26.5	494	88	(0.19, 0.40)
HCB-2-20 wt%	4.4	22.4/12.4/5.0	44.2	28.3	496	92	(0.23, 0.39)
HCB-2-30 wt%	4.3	14.9/10.6/4.8	39.1	25.1	500	91	(0.21, 0.43)
HCB-2-100 wt%	4.9	14.8/8.3/3.7	40.6	23.6	512	95	(0.24, 0.48)

[a] Turn-on voltage. [b] Maximum EQE, and values at 100 and 1000 cd/m^2. [c] $EQE_{roll\text{-}off}$ = $(EQE_{max}\text{-}EQE_{100/1000})/EQE_{max}$ [d] Maximum CE and PE. [e] EL peak, FWHM and CIE color coordinates.

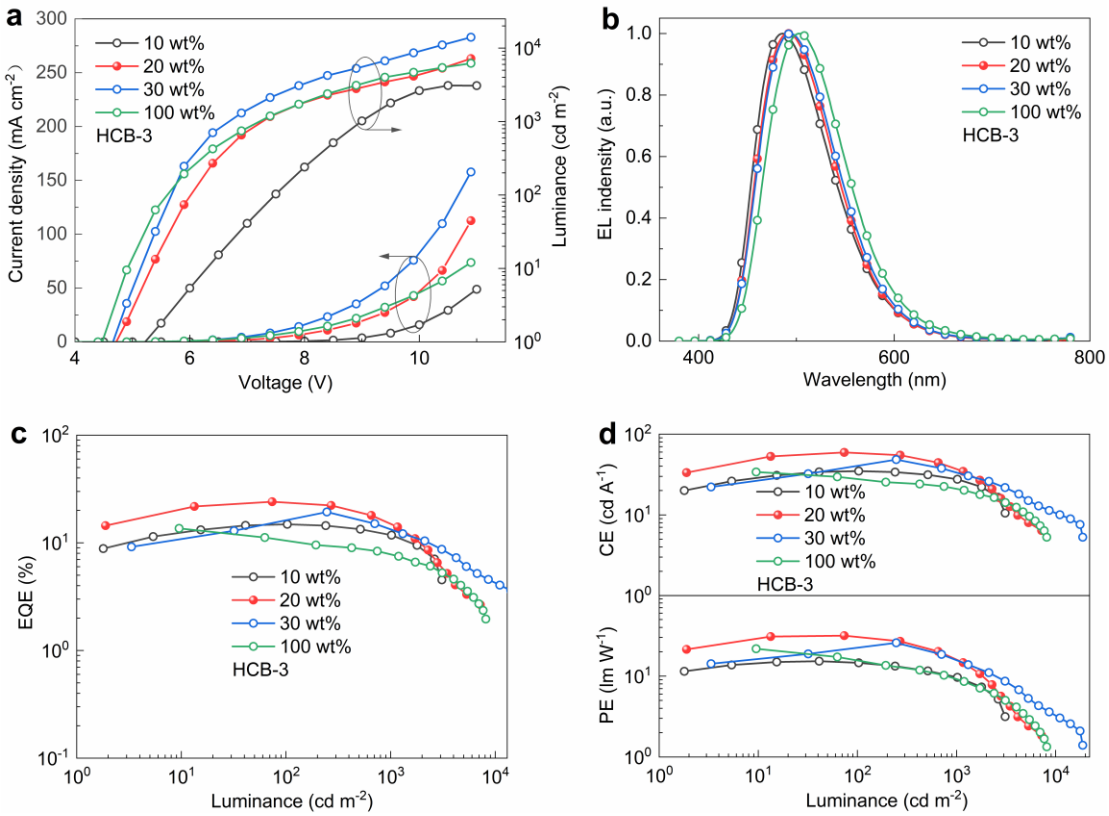

Fig. S32 Device Performance of HCB-3. a) *J-V-L* curves, b) EL spectra. c) EQE as a function of luminance. d) PE and CE as a function of luminance.

Table S8. OLEDs performance based on HCB-3.

EML	V_{on}[a] [V]	EQE[b] [%]	CE[c] [cd A^{-1}]	PE[d] [lm W^{-1}]	λ_{EL}[e] [nm]	FWHM[e] [nm]	CIE[e] (x, y)
HCB-3-10 wt%	5.2	14.8/14.5/11.7	34.8	15.2	486	87	(0.18, 0.37)
HCB-3-20 wt%	4.7	24.1/23.7/15.2	59.4	31.6	492	87	(0.19, 0.39)
HCB-3-30 wt%	4.6	19.3/16.2/13.2	48.3	25.7	494	87	(0.19, 0.41)
HCB-3-100 wt%	4.4	13.6/10.5/7.8	34.0	21.8	502	89	(0.20, 0.44)

[a] Turn-on voltage. [b] Maximum EQE, and values at 100 and 1000 cd/m^2. [c] $EQE_{roll\text{-}off}$ = $(EQE_{max}\text{-}EQE_{100/1000})/EQE_{max}$ [d] Maximum CE and PE. [e] EL peak, FWHM and CIE color coordinates.

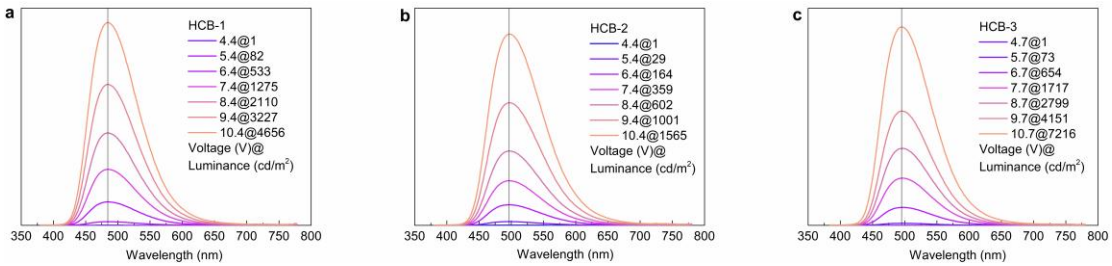

Fig. S33 The EL characteristics of a) HCB-1, b) HCB-2, and c) HCB-3 under different voltages and brightness levels.

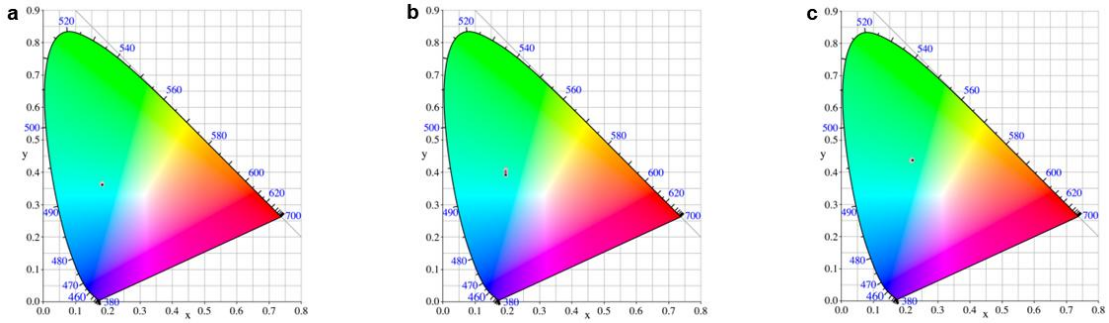

Fig. S34 The CIE coordinates of a) HCB-1 (4.4~10.4 V), b) HCB-2 (4.4~10.4 V), and c) HCB-3 (4.7~10.7 V) under different voltages and brightness levels.

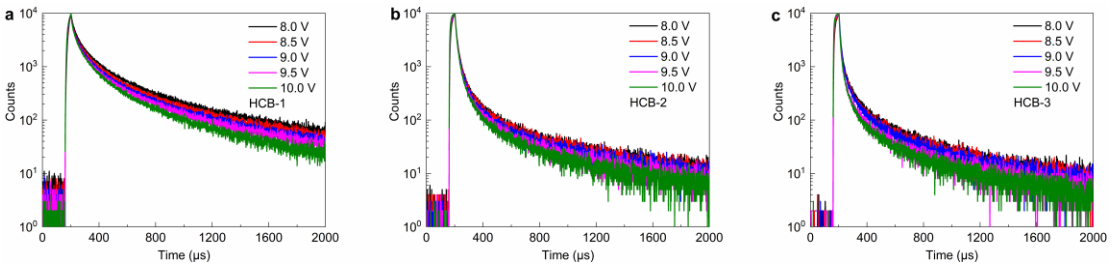

Fig. S35 Transient EL spectra at 1000 cd m^{-2} of device HCB 1-3.

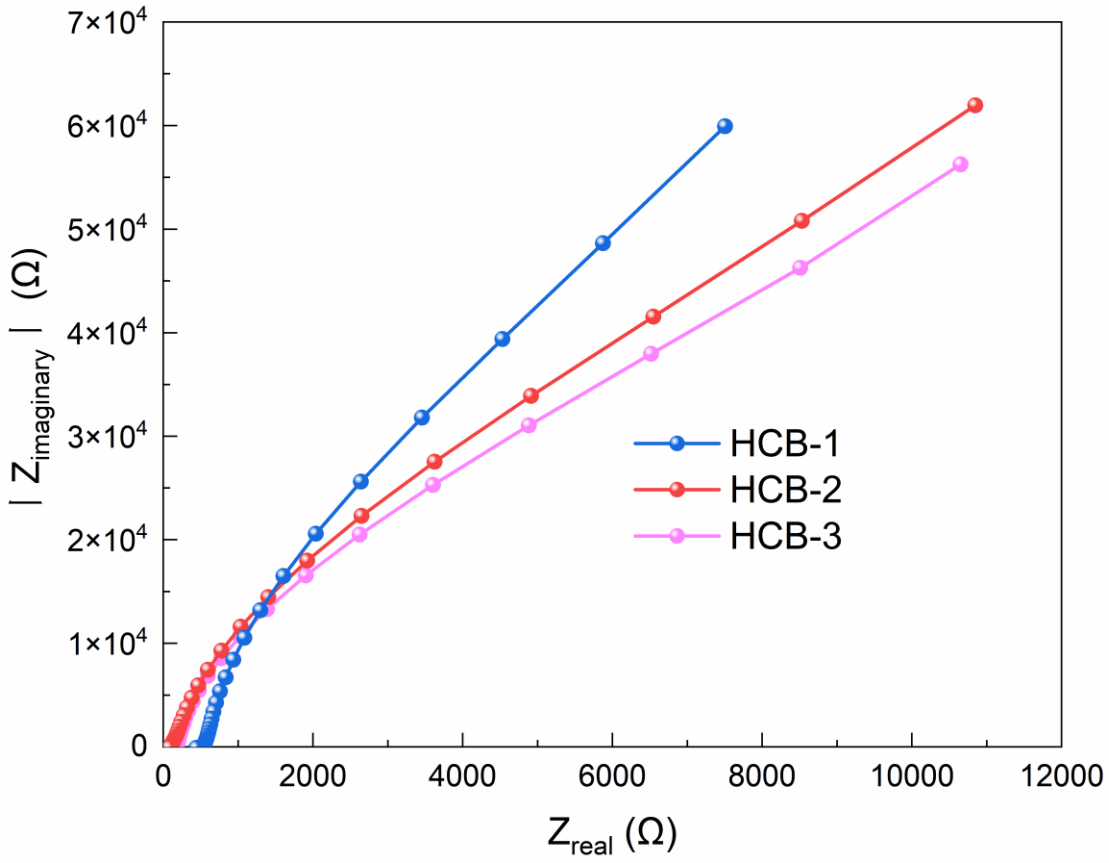

Fig. S36 EIS measurement of different devices.

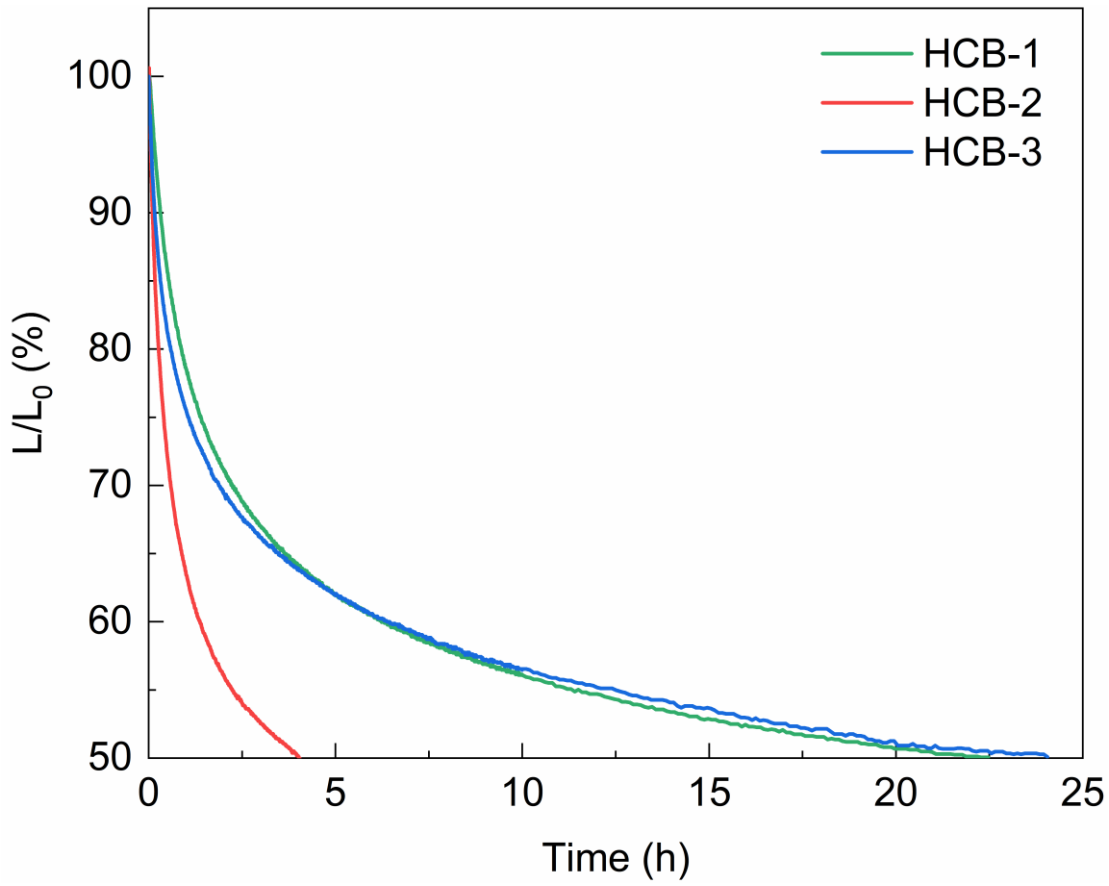

Fig. S37 The operation lifetime of the devices (at an initial luminance of 100 cd m^{-2}). L, luminance of the device during the operational lifetime measurement; L_0, initial luminance of the device.

Table S9. EL performances of the reported blue and sky blue TADF-OLEDs by solution process.

Emitters	V_{on}[a] (V)	EQE_{max}[b] (%)	EQE_{100}[b] (%)	EQE_{1000}[b] (%)	$EQE_{roll\text{-}off}$[c] (%)	λ_{EL}[d] (nm)	Ref.
HCB-1	**4.3**	**21.0**	**17.6**	**9.4**	**16.1/55.2**	**486**	**This work**
HCB-2	**4.4**	**22.4**	**12.4**	**5.0**	**44.6/77.6**	**496**	**This work**
HCB-3	**4.7**	**24.1**	**23.7**	**15.2**	**1.7/36.9**	**492**	**This work**
TPA-s-Mes*B	4.0	10.3	7.8	-	24.2/-	454	1
Without PFN-Br	4.8	17.5	13.6	-	22.2/-	473	2
0.2 mg/ml PFN-Br	4.5	21.2	19.3	-	8.9/-	473	2
0.5 mg/ml PFN-Br	4.8	10.4	7.78	-	25.1/-	473	2
TTT-Ph-Ac	4.4	23.23	-	-	-/-	492	3
B-oCz	4.4	8.0	6.9	2.6	13.7/67.5	463	4
B-oTC	3.9	19.1	17.0	9.7	11.0/49.2	474	4
DCzIPN	5.1	9.5	-	7.6	-/20.0	466	5
DMeCzIPN	3.8	21.6	-	19.6	-/9.2	478	5
T-CNDF-T-tCz	6.3	21.0	-	-	-/-	484	6
4CzFCN	3.6	21.0	20.2	13.6	3.8/35.2	480	7
MeCz-4CzCN	2.9	21.8	21.3	19.0	2.2/12.8	486	8
PhCz-4CzCN	2.9	20.6	20.0	18.2	2.9/11.6	475	8
PhDCz-4CzCN	3.1	10.0	9.8	7.9	2.0/21.0	465	8
PMB-SPAc	3.6	26.04	21.94	-	15.7/-	492	9
CzDMAC-DPS	3.6	12.2	6.9	4.5	43.4/63.1	492	10
DCzDMAC-DPS	5.2	2.2	1.5	-	31.8/-	464	10

[a] Turn-on voltage at 1 cd/m^2. [b] EQE at maximum, 100 cd/m^2, and 1000 cd/m^2. [c] $EQE_{roll\text{-}off} = (EQE_{max}\text{-}EQE_{100/1000})/EQE_{max}$ [d] EL peak.

Table S10. EL performances of the reported blue and sky blue TADF-OLEDs for vacuum-deposited devices.

Emitters	V_{on}[a] (V)	EQE_{max}[b] (%)	EQE_{100}[b] (%)	EQE_{1000}[b] (%)	$EQE_{roll\text{-}off}$[c] (%)	Lifetime[d] (h)	λ_{EL}[e] (nm)	Ref.
HCB-1	**4.3**	**21.0**	**17.6**	**9.4**	**16.1/55.2**	**LT_{50}@100=22.4**	**486**	**This work**
HCB-2	**4.4**	**22.4**	**12.4**	**5.0**	**44.6/77.6**	**LT_{50}@100=4.0**	**496**	**This work**
HCB-3	**4.7**	**24.1**	**23.7**	**15.2**	**1.7/36.9**	**LT_{50}@100=24.0**	**492**	**This work**
BN-C	2.6	22.3	21.7	15.8	2.7/29.1	LT_{50}@1000=33.5	477	[11]
BN-Si	2.6	23.2	23.2	21.7	-/6.5	LT_{50}@1000=428.6	477	[11]
BN-Ge	2.6	21.2	21.1	19.1	0.4/9.9	LT_{50}@1000=98.9	473	[11]
BN-Si[k]	2.7	25.3	24.6	21.4	2.7/15.4	LT_{50}@1000=308	476	[11]
B1	3.8	32.5	16.8	6.5	48/80	-	450	[12]
B2	3.3	30.1	17.8	8.5	40.8/71.7	-	452	[12]
DPA-B2	3.6	28.9	19.8	9.3	31.4/67.8	LT_{50}@100=137.1	444	[13]
DPA-B3	3.6	37.7	33.7	21.0	10.6/44.2	LT_{50}@100=317.3	450	[13]
DPA-B4	3.6	39.2	36.4	28.7	7.1/26.7	LT_{50}@100=418.0	457	[13]
Cz-B4	3.6	32.1	26.9	16.1	16.2/49.8	LT_{50}@100=777.4	457	[13]
DPA-B4 (HF)	3.6	44.4	44.3	38.8	0.2/12.6	LT_{50}@100=409.6	459	[13]
TSF-A	-	29.2	-	24.1	-/17.4	LT_{80}@1000=398	468	[14]
TSF-B	-	33.1	-	29.0	-/12.3	LT_{80}@1000=1365	468	[14]
TSF-C	-	28.2	-	21.3	-/24.4	LT_{80}@1000=126	468	[14]
TSF-D	-	30.4	-	27.2	-/10.5	LT_{80}@1000=561	468	[14]
4tCzBN-PhCN		37.1	-	34.2	-/1.8	LT_{95}@5000=37.6	501	[15]
4CzBN-PhCN		28.0	-	26.6	-/5.0	LT_{95}@5000=26.7	489	[15]

[a] Turn-on voltage at 1 cd/m^2. [b] EQE at maximum, 100 cd/m^2, and 1000 cd/m^2. [c] $EQE_{roll\text{-}off} = (EQE_{max}\text{-}EQE_{100/1000})/EQE_{max.}$ [e] where LT_x@y indicates the time to reach x% of the initial luminance of y cd m^{-2} [e] EL peak.

References

1 G. Liao, J. Lei, S. Li, M. Liu, Y. Qiao, K. Liu, N. Wang, Q. Niu and X. Yin, *Adv. Opt. Mater.*, 2024, **12**, 2301242.

2 M. Li, J. Jiang, Y. Ning, S. Zhao, W.F.A. Masri, S. Wageh and A. Al-Ghamdi, Synth. Met., 2022, **289**, 117122.

3 X. Chen, S. Wang, H.L. Lee, J.Y. Lee, X. Liao, L. Li, W. Zhu and Y. Wang, Adv. Opt. Mater., 2021, **9**, 2101518.

4 X.-L. Chen, J.-H. Jia, R. Yu, J.-Z. Liao, M.-X. Yang and C.-Z. Lu, Angew. Chem., Int. Ed., 2017, **56**, 15006-15009.

5 G. Kreiza, D. Berenis, D. Banevičius, S. Juršėnas, T. Javorskis, E. Orentas and K. Kazlauskas, Chem. Eng. J., 2021, **412**, 128574.

6 X. Zheng, R. Huang, C. Zhong, G. Xie, W. Ning, M. Huang, F. Ni, F.B. Dias and C. Yang, Adv. Sci., 2020, **7**, 1902087.

7 Z. He, C. Wang, J. Zhao, X. Du, H. Yang, P. Zhong, C. Zheng, H. Lin, S. Tao and X. Zhang, J. Mater. Chem. C, 2019, **7**, 11806-11812.

8 X. Ban, F. Chen, J. Pan, Y. Liu, A. Zhu, W. Jiang and Y. Sun, Chem. Eur. J, 2020, **26**, 3090-3102.

9 B. Li, Z. Ding, Z. Wu, M. Liu, S. Chen, D. Chen, Z. Li, L. Sang, Y. Liu, L. Lin, W. Zhu and X. Wan, Chem. Eng. J., 2023, **476**, 146484.

10 J. Luo, S. Gong, Y. Gu, T. Chen, Y. Li, C. Zhong, G. Xie and C. Yang, J. Mater. Chem. C, 2016, **4**, 2442-2446.

11 S.-J. Li, X. Tang, C. H. Ng, J. Y. Lim, W. K. Tang, W.-C. Chen, Y. Huo, M. Ng, S. S. Chen, D. Zhang, L. Duan and M.-C. Tang, Adv. Optical Mater., 2025, 2402479.

12 Y. Mei, J. Li, D. Liu, M. Xu, Y. Li and H. Wan, Adv. Optical Mater., 2024, 2402964.

13 T. Hua, X. Cao, J. Miao, X. Yin, Z. Chen, Z. Huang and C. Yang Nat. Photon.2024, **18**, 1161–1169

14 T. Huang, Q. Wang, H., Y. Zhang, G. Zhan, D. Zhang and L. Duan, Nat. Photon. 2024, **18**, 516–523

15 T. Huang, Q. Wang, H. Zhang, Y. Xin, Y. Zhang, X. Chen, D. Zhang and L. Duan, Nat. Mater. 2024, **23**, 1523–1530.